

Article

Powders Synthesized from Solutions of Calcium Chloride, Sodium Hydrogen Phosphate, and Sodium Sulfate for Bioceramics Production

Tatiana V. Safronova ^{1,2,*}, Alexander S. Khantimirov ¹, Tatiana B. Shatalova ^{1,2}, Yaroslav Y. Filippov ^{2,3}, Irina V. Kolesnik ^{1,2} and Alexander V. Knotko ²

¹ Department of Chemistry, Lomonosov Moscow State University, Building, 3, Leninskie Gory, 1, 119991 Moscow, Russia

² Department of Materials Science, Lomonosov Moscow State University, Building, 73, Leninskie Gory, 1, 119991 Moscow, Russia

³ Research Institute of Mechanics, Lomonosov Moscow State University, Michurinsky Pr., 1, 119192 Moscow, Russia

* Correspondence: safronovatv@my.msu.ru; Tel.: +7-916-3470641

Abstract: Fine powders of brushite $\text{CaHPO}_4 \cdot 2\text{H}_2\text{O}$, ardealite $\text{Ca}(\text{HPO}_4)_x(\text{SO}_4)_{1-x} \cdot 2\text{H}_2\text{O}$ ($\text{Ca}(\text{HPO}_4)_{0.5}(\text{SO}_4)_{0.5} \cdot 2\text{H}_2\text{O}$), and calcium sulfate dihydrate $\text{CaSO}_4 \cdot 2\text{H}_2\text{O}$ —all containing sodium chloride NaCl as a reaction by-product—were synthesized from 0.5M aqueous solution of calcium chloride CaCl_2 , sodium hydrophosphate Na_2HPO_4 and/or sodium sulfate Na_2SO_4 . Powder of ardealite $\text{Ca}(\text{HPO}_4)_x(\text{SO}_4)_{1-x} \cdot 2\text{H}_2\text{O}$ ($\text{Ca}(\text{HPO}_4)_{0.5}(\text{SO}_4)_{0.5} \cdot 2\text{H}_2\text{O}$) was synthesized by precipitation from aqueous solution of calcium chloride CaCl_2 and mixed-anionic solution simultaneously containing the hydrogen phosphate anion HPO_4^{2-} (Na_2HPO_4) and sulfate anion SO_4^{2-} (Na_2SO_4). Sodium chloride NaCl, presenting in compacts based on synthesized powders of brushite $\text{CaHPO}_4 \cdot 2\text{H}_2\text{O}$, ardealite $\text{Ca}(\text{HPO}_4)_x(\text{SO}_4)_{1-x} \cdot 2\text{H}_2\text{O}$ ($\text{Ca}(\text{HPO}_4)_{0.5}(\text{SO}_4)_{0.5} \cdot 2\text{H}_2\text{O}$) and calcium sulfate dihydrate $\text{CaSO}_4 \cdot 2\text{H}_2\text{O}$, was responsible for both low-temperature melt formation and the creation of phase composition of ceramics. Heterophase interaction of components led to the resulting phase composition of the ceramic samples during heating, including the formation of chlorapatite $\text{Ca}_5(\text{PO}_4)_3\text{Cl}$ in powders of brushite and ardealite. The phase composition of the ceramics based on the powder of brushite $\text{CaHPO}_4 \cdot 2\text{H}_2\text{O}$ containing NaCl as a by-product after firing at 800–1000 °C included $\beta\text{-Ca}_2\text{P}_2\text{O}_7$, and $\text{Ca}_5(\text{PO}_4)_3\text{Cl}$. The phase composition of ceramics based on the powder of ardealite $\text{Ca}(\text{HPO}_4)_x(\text{SO}_4)_{1-x} \cdot 2\text{H}_2\text{O}$ ($\text{Ca}(\text{HPO}_4)_{0.5}(\text{SO}_4)_{0.5} \cdot 2\text{H}_2\text{O}$) containing NaCl as a by-product after firing at 800 and 900 °C included $\beta\text{-Ca}_2\text{P}_2\text{O}_7$, CaSO_4 , and $\text{Ca}_5(\text{PO}_4)_3\text{Cl}$; after firing at 1000 °C, it included CaSO_4 , $\text{Ca}_5(\text{PO}_4)_3\text{Cl}$ and $\text{Ca}_3(\text{PO}_4)_2/\text{Ca}_{10}\text{Na}(\text{PO}_4)_7$, and after firing at 1100 °C, it included CaSO_4 and $\text{Ca}_5(\text{PO}_4)_3\text{Cl}$. The phase composition of ceramics based on powder of calcium sulfate dihydrate $\text{CaSO}_4 \cdot 2\text{H}_2\text{O}$ containing NaCl as a by-product after firing at 800–1100 °C included CaSO_4 as the predominant phase. The phase composition of all ceramic samples under investigation consisted of biocompatible crystalline phases with different abilities to biodegrade. For this reason, the created ceramics can be recommended for testing as materials for treatment of bone defects using regenerative medicine methods.

Keywords: brushite; calcium sulfate dihydrate; mixed-anionic solution; ardealite; sodium chloride; calcium pyrophosphate; chlorapatite; calcium sulfate anhydrite



Citation: Safronova, T.V.; Khantimirov, A.S.; Shatalova, T.B.; Filippov, Y.Y.; Kolesnik, I.V.; Knotko, A.V. Powders Synthesized from Solutions of Calcium Chloride, Sodium Hydrogen Phosphate, and Sodium Sulfate for Bioceramics Production. *Ceramics* **2023**, *6*, 561–583. <https://doi.org/10.3390/ceramics6010034>

Academic Editor: Sergey Mjakin

Received: 31 December 2022

Revised: 28 January 2023

Accepted: 15 February 2023

Published: 22 February 2023



Copyright: © 2023 by the authors. Licensee MDPI, Basel, Switzerland. This article is an open access article distributed under the terms and conditions of the Creative Commons Attribution (CC BY) license (<https://creativecommons.org/licenses/by/4.0/>).

1. Introduction

Biocompatible resorbable ceramic materials are currently of considerable interest, especially for the treatment of bone defects using regenerative medicine methods [1,2]. For the implementation of regenerative medicine methods, ideal bone implants placed in bone defects should gradually dissolve in the body environment, providing necessary ions for bone tissue reconstruction and performing its supporting functions, while new bone tissue

should form in its place. The leading place among the variety of biocompatible inorganic materials belongs to those based on calcium phosphates [3]. Additionally, inorganic materials based on calcium carbonates [4–6] and calcium silicates [7–10], calcium sulfates [11–14], or containing calcium sulfates in combinations with calcium phosphates [15–19] have been the focus of investigations.

Since ideal ceramic material for the treatment of bone defects has not yet been created, research on the creation of new biomaterials is ongoing. Biocompatible anions and cations presenting in living organisms, such as HPO_4^{2-} , CO_3^{2-} , SiO_4^{4-} , SO_4^{2-} , Cl^- , Ca^{2+} , Mg^{2+} , Sr^{2+} , Na^+ , K^+ , etc., have inspired the creation of biocompatible materials with tunable properties such as osteoinduction and bioresorbability [20]. Ceramics containing phases of β -calcium pyrophosphate [21,22] and calcium sulfate anhydrite [23–27] could potentially demonstrate both biocompatibility and resorption ability. The phase of calcium sulfate anhydrite CaSO_4 is usually introduced in ceramic materials in order to control the limit and rate of resorption of materials intended for the treatment (temporary compensation) of bone tissue defects in the process of their restoration [28].

To prepare β -calcium pyrophosphate ceramics, the following powder precursors can be used: brushite $\text{CaHPO}_4 \cdot 2\text{H}_2\text{O}$ [29–31], monetite CaHPO_4 [32,33], hydrated calcium pyrophosphate $\text{Ca}_2\text{P}_2\text{O}_7 \cdot x\text{H}_2\text{O}$ [34], calcium pyrophosphate $\text{Ca}_2\text{P}_2\text{O}_7$, and different powder mixtures [35] or calcium phosphate cement stones [36–38] with molar ratio $\text{Ca}/\text{P} = 1$.

To prepare calcium sulfate anhydrite ceramics, the following powder precursors can be used: calcium sulfate dihydrate [23], calcium sulfate hemihydrate [11,12], and calcium sulfate anhydrite [27]. Calcium sulfate hemihydrate is known to be a starting powder for chemically bonded calcium sulfate dihydrate cement stone. Ceramics based on calcium sulfate anhydrite can be obtained via the firing of calcium sulfate dihydrate cement or cement-salt stone, also in the form of 3D-printed pre-ceramic items [39].

To create ceramics with a uniform microstructure and phase arrangement, it is necessary to use fine powders with high sinterability and homogeneity of components. Such fine powders can be prepared via precipitation from solutions and suspensions, including highly loaded ones for the preparation of powder blanks [36–38]. Water solutions of different soluble calcium salts (nitrate, chloride, acetate, lactate, etc.) or water suspensions of fine particles of calcium compounds (hydroxide, citrate, carbonate) with low solubility can be used in both the synthesis of calcium phosphates [32] and the synthesis of calcium sulfates [40]. Water solutions of pyrophosphoric or orthophosphoric acids, or the soluble salts of ammonium, sodium, or potassium of these acids, can be used for the synthesis of calcium phosphates. Water solutions of sulfur acid or soluble ammonium, sodium or potassium sulfates can be used for calcium sulfate syntheses.

From the point of view of high-quality ceramics preparation, in an ideal case, starting powder with an appropriate homogeneity that is characteristic of quasi-amorphous [41,42] or monophase powder should be used. Powder of octacalcium phosphate ($\text{Ca}/\text{P} = 1.33$) is probably a unique example of synthetic monophase powder for the creation of biocompatible composite ceramics [43]. This powder can be used for the preparation of composite bi-phase ceramics containing tricalcium phosphate $\text{Ca}_3(\text{PO}_4)_2$ ($\text{Ca}/\text{P} = 1.5$) and β -calcium pyrophosphate $\beta\text{-Ca}_2\text{P}_2\text{O}_7$ ($\text{Ca}/\text{P} = 1$) [44]. Syntheses from mixed-anionic HPO_4/CO_3 [45–48], $\text{P}_2\text{O}_7/\text{CO}_3$ [49], $\text{HPO}_4/\text{P}_2\text{O}_7$ [50], $\text{HPO}_4/\text{SiO}_3$ [51], CO_3/SO_4 [52], HPO_4/SO_4 [53] or mix-cationic K/Na [54] aqueous solutions make it possible to prepare amorphous powders or powders containing crystalline target and by-product phases with high homogeneity for bioceramics production. Homogeneous powder mixtures can be prepared through the preservation of reaction by-products as components of the powder mixture during synthesis via the precipitation and separation of the precipitate from the mother liquor without washing the precipitate [51,54,55]. Sodium [51,56–58] or potassium [59–62] salts have been reported as the preserved by-products in such powders for the production of bioceramics, as components taking part in the formation of phase composition at further firing stages.

Ardealite $\text{Ca}(\text{HPO}_4)_{0.5}(\text{SO}_4)_{0.5}\cdot 2\text{H}_2\text{O}$ powder can be considered a monophasic highly homogeneous precursor of a ceramic composite material containing phases of calcium pyrophosphate $\text{Ca}_2\text{P}_2\text{O}_7$ and calcium sulfate anhydrite CaSO_4 . To synthesize powder of ardealite $\text{Ca}(\text{HPO}_4)_{0.5}(\text{SO}_4)_{0.5}\cdot 2\text{H}_2\text{O}$ via precipitation, different combinations of starting salts or other compounds can be used. These combinations should include soluble calcium compounds (above all, salts), as well as soluble sulfates and phosphates. For example, in order to characterize the mineral, ardealite has been synthesized from 0.5 M aqueous solution CaCl_2 and $\text{Na}_2\text{HPO}_4/(\text{NH}_4)_2\text{SO}_4$ [63,64]. Ardealite has also been synthesized using $\text{Ca}(\text{OH})_2$, $\text{Na}_2\text{HPO}_4\cdot 12\text{H}_2\text{O}$, and Na_2SO_4 as starting materials [65]. The link between brushite $\text{CaHPO}_4\cdot 2\text{H}_2\text{O}$ and gypsum $\text{Ca}(\text{SO}_4)_2\cdot 2\text{H}_2\text{O}$ and the possibility of formation of solid solutions based on ardealite have been studied during synthesis from aqueous solution of Na_2SO_4 and H_3PO_4 of different concentrations and at different $\text{SO}_4^{2-}/\text{HPO}_4^{2-}$ ratios [66]. These solutions were mixed with each other in the molar ratio of $\text{Ca}/(\text{P} + \text{S}) = 1$. Ardealite can be synthesized as a mineral of cement stone prepared from a powder mixture of β -tricalcium phosphate $\text{Ca}_3(\text{PO}_4)_2$ and calcium sulfate hemihydrate $\text{CaHPO}_4\cdot 0.5\text{H}_2\text{O}$ [67]. Additional information about crystal structure of ardealite can be found in articles devoted to construction materials and minerals present in nature [68,69].

In a series of earlier studies [45,49–51] we showed that synthesis from mixed-anionic solutions makes it possible to prepare an amorphous powder with proper homogeneity of distribution of precursors of high-temperature phases in ceramic material. In this research, we further develop the considered approach in respect to the synthesis of powder from mixed-anionic solution containing HPO_4^{2-} and SO_4^{2-} anions.

As shown in our previous studies [51,54–62], preservation of by-products in the synthesized powder can also be treated as an approach through which to achieve good homogeneity of starting components in powder mixture. In a continuation of this research, this paper presents the considered approach in respect to preservation of NaCl as reaction by-product in the synthesized powders.

It should be noted that due to crystal structure identity synthesis from mixed-anionic solution containing HPO_4^{2-} and SO_4^{2-} anions makes it possible to prepare monophasic mineral ardealite. The advantages of ardealite, as a monophasic powder with a highly uniform distribution of precursors of phases of biocompatible and bioresorbable ceramics such as β -calcium pyrophosphate $\beta\text{-Ca}_2\text{P}_2\text{O}_7$ and calcium sulfate anhydrite CaSO_4 , have still not been leveraged or reported on in studies published to date. The aim of this investigation consisted of the synthesis of ardealite powder for production of ceramics including biocompatible and bioresorbable phases of β -calcium pyrophosphate $\beta\text{-Ca}_2\text{P}_2\text{O}_7$ and calcium sulfate anhydrite CaSO_4 . Solutions of calcium chloride CaCl_2 , sodium hydrogen phosphate Na_2HPO_4 , and sodium sulfate Na_2SO_4 were used in present investigation. The above-mentioned approach of preserving reaction by-products (NaCl in this work) in synthesized powder as a method to prepare the starting homogeneous powder mixture for ceramics production was also used. All ions intended to take part in the powder synthesis and ceramics preparation were biocompatible. In addition, this fact gave us the hope of preparing new biocompatible ceramic materials for treatment of bone defects.

2. Materials and Methods

2.1. Powders and Ceramic Samples Preparation

Water solutions of calcium chloride CaCl_2 ($\text{CaCl}_2\cdot 6\text{H}_2\text{O}$, CAS No.: 7774-34-7, Sigma-Aldrich, St. Louis, MO, USA, puriss. p.a. $\geq 98\%$), sodium sulfate Na_2SO_4 (CAS No.: 7757-82-6, Sigma-Aldrich, St. Louis, MO, USA, puriss. p.a. $\geq 99\%$), and sodium hydrophosphate Na_2HPO_4 (CAS No.: 7558-79-4, Sigma-Aldrich, St. Louis, MO, USA, puriss. p.a. $\geq 99\%$) were used for the syntheses of powders. Labeling of syntheses, concentrations of solutions, volumes of solutions, and molar ratios of components used in each synthesis are presented in Table 1.

Table 1. Synthesis conditions and labeling of the samples.

Labeling of the Samples (Solutions, Powders, Ceramics)	Concentrations and Volumes of Aqueous Solutions					Molar Ratio of Salts in the Synthesis
	Ca-Containing Solution		Na-Containing Solution			
	CaCl ₂	Volume	Na ₂ HPO ₄	Na ₂ SO ₄	Volume	
PO4	0.5 M	300 mL	0.5 M	0	300 mL	[CaCl ₂]/[Na ₂ HPO ₄] = 1:1
PO4_SO4	0.5 M	300 mL	0.25 M	0.25 M	300 mL	[CaCl ₂]/[Na ₂ HPO ₄]/[Na ₂ SO ₄] = 1:0.5:0.5
SO4	0.5 M	300 mL	0	0.5 M	300 mL	[CaCl ₂]/[Na ₂ SO ₄] = 1:1

The synthesis of the powders was carried out at room temperature. Solutions of the sodium salts (Na₂HPO₄, Na₂HPO₄/Na₂SO₄, Na₂SO₄) were poured into solutions of calcium chloride CaCl₂. The resulting suspensions of precipitate in the mother liquors after the addition of Na⁺ solutions were kept in the magnetic stirrer for a period of 30 min. The precipitates were filtered out on the Buchner funnel under reduced pressure. After filtration synthesized products were dried by evenly distributing in a thin layer over the surface of plastic trays for seven days in the air at room temperature. The mother liquors were also collected and dried for isolation and investigation of the reaction by-products.

Then, after drying, synthesized powders PO4, PO4_SO4, SO4 were disaggregated in a planetary mill (Fritch Pulverisette, Idar-Oberstein, Germany) in acetone medium for 15 min at a rotation speed of 600 rpm. Containers and grinding media made from zirconia were used. Then, 10 g of powder and 50 g of grinding media were taken for each sample. After acetone evaporated dry powders were passed through the sieve with 200 µm mesh.

Pre-ceramic powder compacts in the form of discs with a diameter of 12 mm and a height of 2–3 mm were made from a prepared powders using a steel mold and a manual press (Carver Laboratory Press model C, Fred S. Carver, Inc., Wabash, IN, USA) at 100 MPa. Then, pre-ceramic powder compacts were fired in the air in a furnace at 800 °C, 900 °C, 1000 °C, and 1100 °C, with exposure at the specified temperatures for 2 h (the heating rate of the furnace was 5 °C/min).

2.2. Characterization of Samples

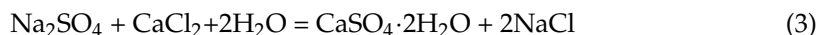
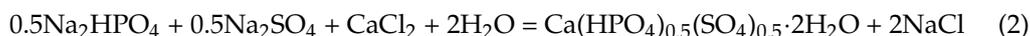
The bulk density of the powders after synthesis and after disaggregation was determined as mass of 1 cm³ of powder volume. Density of green powder compacts and sintered ceramic samples was calculated from the measured mass and volume based on geometry dimensions of the specimens. The phase composition of the powders after synthesis, powders after disaggregation and ceramic samples after heat treatment at 800 °C, 900 °C, 1000 °C, and 1100 °C was determined by X-ray powder diffraction (XRD) analysis using a Rigaku D/MAX 2500 diffractometer (Rigaku Corporation, Tokyo, Japan), CuKα radiation, with an angle interval 2θ from 2° to 70° (step 2θ = 0.02°). Phase analysis was performed using the ICDD PDF2 database [70] and Match! software (<https://www.crystalimpact.com/>, accessed on 11 February 2023). The content of phases in products isolated from the mother liquor was determined using Match! software. Infrared spectra were collected using Spectrum Three FTIR spectrometer (Perkin Elmer, Waltham, MA, USA) in attenuated total reflectance mode in the wavenumber range of 520–4000 cm⁻¹ with Universal ATR accessory (diamond/KRS-5 crystal). The bands in spectra were attributed on the basis of the literature [71]. Thermal analysis (TA) was performed to determine the total mass loss of the synthesized powders at heating up to 1000 °C in the air using Netzsch STA 409 PC Luxx thermal analyzer (NETZSCH, Selb, Germany). The sample weight was at least 10 mg. The gas phase composition was monitored by the quadrupole mass spectrometer QMS 403 Quadro (NETZSCH, Selb, Germany) combined with a thermal analyzer Netzsch STA 409 PC Luxx. The mass spectra (MS) were registered for the following m/Z values: 18 (H₂O); 64 (SO₂); the heating rate was 10 °C/min. The thermogravimetric weight loss curve (TG, mg) and the weight loss derivative curve (DTG, arb. units) were recorded as a function of time and temperature. The specimens' microstructure was studied using a SUPRA

50 VP scanning electron microscope (Carl Zeiss, Oberkochen, Germany); the imaging was performed in a low vacuum mode at an accelerating voltage of 3–21 kV (SE2 detector). The surface of the powders and ceramics was coated with a layer of chromium (up to 10 nm).

3. Results and Discussion

According to XRD data (Figure 1a), the phase composition of powder PO4 synthesized from calcium chloride CaCl_2 and sodium hydrophosphate Na_2HPO_4 consisted of brushite $\text{CaHPO}_4 \cdot 2\text{H}_2\text{O}$ (card PDF 21-816) as the dominating phase, and monetite CaHPO_4 (card PDF 9-80) and sodium chloride NaCl (card PDF 5-628). The phase composition of powder SO4 synthesized from calcium chloride CaCl_2 and sodium sulfate Na_2SO_4 consisted of calcium sulfate dihydrate $\text{CaSO}_4 \cdot 2\text{H}_2\text{O}$ and sodium chloride NaCl . The phase composition of powder PO4_SO4 synthesized from CaCl_2 and mixed-anionic solution of sodium hydrophosphate Na_2HPO_4 and sodium sulfate Na_2SO_4 consisted of hydrated mixed calcium phosphate sulfate $\text{Ca}(\text{HPO}_4)_x(\text{SO}_4)_{1-x} \cdot 2\text{H}_2\text{O}$ (according WinXPow, card PDF 46-657) or ardealite $\text{Ca}(\text{HPO}_4)_{0.5}(\text{SO}_4)_{0.5} \cdot 2\text{H}_2\text{O}$ (according to Match, card 96-900-0654) and sodium chloride NaCl . The XRD graphs of brushite $\text{CaHPO}_4 \cdot 2\text{H}_2\text{O}$ and calcium sulfate dihydrate $\text{CaSO}_4 \cdot 2\text{H}_2\text{O}$ look very much similar, and this can be treated as a sign of a well-known similarity of their crystal structures. 2θ for 100% peaks of these minerals are also very close (Figure 1b): 11.73 for $\text{CaHPO}_4 \cdot 2\text{H}_2\text{O}$, 11.84 for $\text{CaSO}_4 \cdot 2\text{H}_2\text{O}$ and 11.59 for $\text{Ca}(\text{HPO}_4)_x(\text{SO}_4)_{1-x} \cdot 2\text{H}_2\text{O}$ ($\text{Ca}(\text{HPO}_4)_{0.5}(\text{SO}_4)_{0.5} \cdot 2\text{H}_2\text{O}$). Therefore, the synthesis of ardealite can take place when mixed-anionic solution containing SO_4^{2-} and HPO_4^{2-} is used.

The chemical reactions ((1)–(3)) taking place during synthesis are presented below.

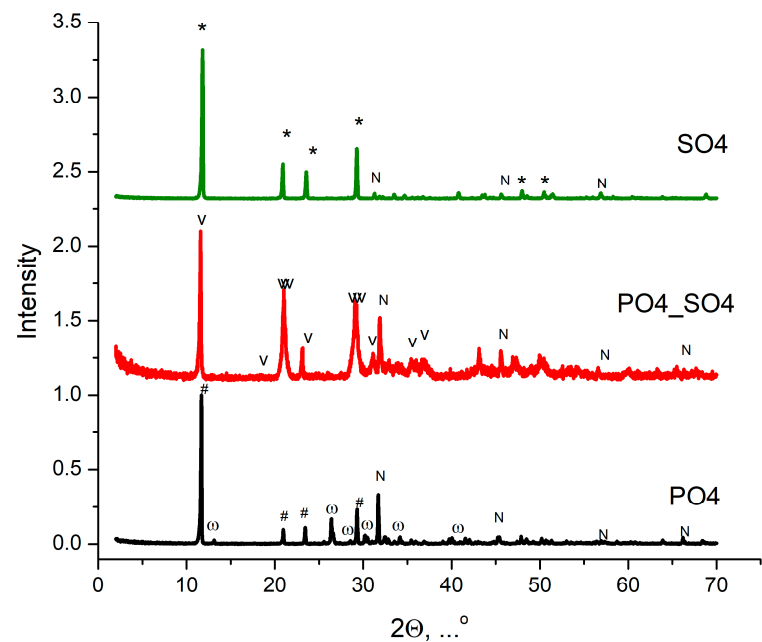


XRD data of products isolated from mother liquors are presented in Figure 2.

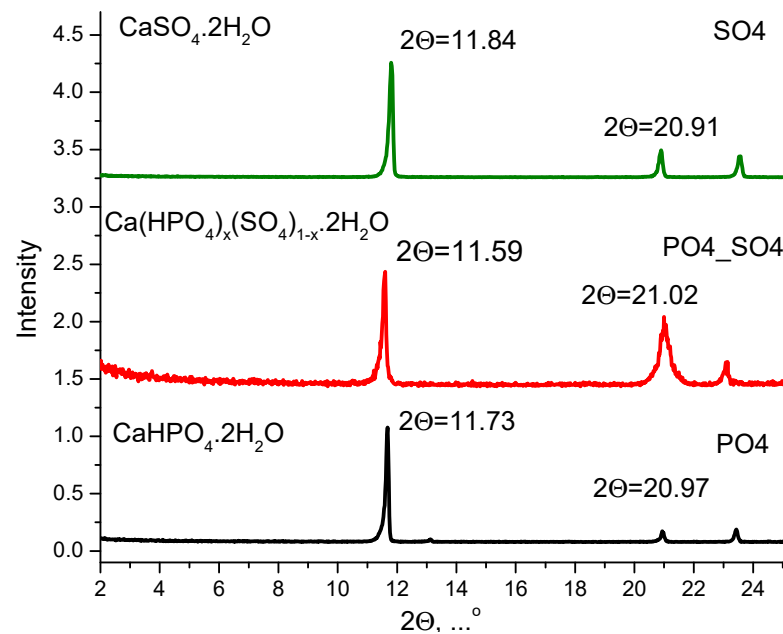
According to the XRD data, the products isolated from the mother liquors (Figure 2) of synthesis by means of Reaction (1) between aqueous solutions of CaCl_2 and Na_2HPO_4 consisted of sodium chloride NaCl ; those isolated from the mother liquor of synthesis by means of Reaction (2) between aqueous solutions of CaCl_2 and $\text{Na}_2\text{HPO}_4/\text{Na}_2\text{SO}_4$ consisted of sodium chloride NaCl (89.9 wt.%) and $\text{CaSO}_4 \cdot 2\text{H}_2\text{O}$ (11.1 wt.%); and those isolated from the mother liquor of synthesis by means of Reaction (3) between aqueous solutions of CaCl_2 and Na_2SO_4 consisted of sodium chloride NaCl (54.8 wt.%) and $\text{CaSO}_4 \cdot 2\text{H}_2\text{O}$ (45.2 wt.%). The composition of products isolated from the mother liquors were estimated using Match! software (Table 2).

The presence of $\text{CaSO}_4 \cdot 2\text{H}_2\text{O}$ in products isolated from the mother liquors PO4_SO4 and SO4 can be explained by the quite good solubility of this mineral in water [72]. The soluble products present in the mother liquor can be retained on the surface of the particles of insoluble products formed during synthesis, or can be occluded in the space between synthesized particles at the stage of filtration. The presence of $\text{CaSO}_4 \cdot 2\text{H}_2\text{O}$ in products isolated from PO4_SO4 mother liquor indicates the slight deviation from the set molar ratio value of $[\text{PO}_4]/[\text{SO}_4] = 1$ determined according to Reaction (2). The possibility of achieving solid solutions based on ardealite has been discussed previously as being possible in both the sulfate-rich and phosphate-rich regions of the composition [66].

The XRD data of synthesized powders after disaggregation in acetone are presented in Figure 3.



(a)



(b)

Figure 1. XRD for 2θ in interval of $2\text{--}70^\circ$ (a) and fragment of XRD for 2θ in interval of $2\text{--}25^\circ$ (b) of powders synthesized from aqueous solution of CaCl_2 and Na_2SO_4 (in green); from CaCl_2 and mixed-anionic solution of $\text{Na}_2\text{HPO}_4/\text{Na}_2\text{SO}_4$ (in red); from CaCl_2 and Na_2HPO_4 , (in black): *— $\text{CaSO}_4 \cdot 2\text{H}_2\text{O}$ (card PDF 21-816); N— NaCl (card PDF 5-628); v— $\text{Ca}(\text{HPO}_4)_x(\text{SO}_4)_{1-x} \cdot 2\text{H}_2\text{O}$ (card PDF 46-657); $\text{Ca}(\text{HPO}_4)_{0.5}(\text{SO}_4)_{0.5} \cdot 2\text{H}_2\text{O}$ (card Match 96-900-0654); #— $\text{CaHPO}_4 \cdot 2\text{H}_2\text{O}$ (card PDF 9-77); ω — CaHPO_4 (card PDF 9-80).

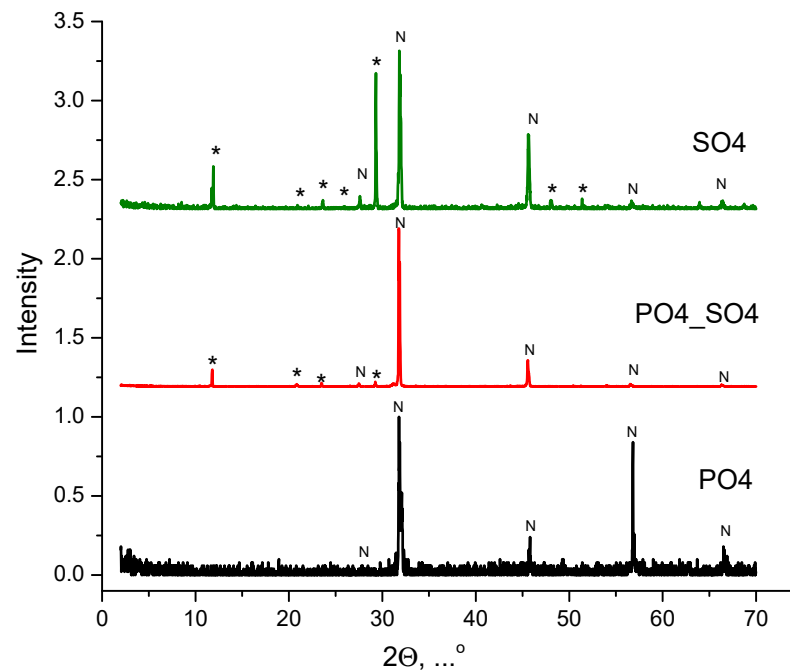


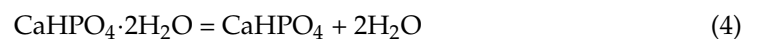
Figure 2. XRD data of products isolated from mother liquors formed during synthesis from aqueous solution of calcium chloride CaCl_2 and sodium sulfate Na_2SO_4 (green line); from aqueous solution of calcium chloride CaCl_2 and sodium hydrophosphate Na_2HPO_4 (black line); as well as from aqueous solution of calcium chloride CaCl_2 and mixed-anionic solution $\text{Na}_2\text{HPO}_4/\text{Na}_2\text{SO}_4$ (red line): *— $\text{CaSO}_4 \cdot 2\text{H}_2\text{O}$ (card PDF 21-816); N— NaCl (card PDF 5-628).

Table 2. The composition of the products isolated from the mother liquors after separation of the precipitate, wt. % **.

Sample	NaCl	$\text{CaSO}_4 \cdot 2\text{H}_2\text{O}$
PO4	100.0	-
PO4_SO4	89.9	11.1
SO4	54.8	45.2

** Match! software (<https://www.crystalimpact.com/>, accessed on 11 February 2023) was used.

The phase composition of the PO4_SO4 and SO4 powders did not change, and included, in addition to sodium chloride NaCl, ardealite $\text{Ca}(\text{HPO}_4)_{0.5}(\text{SO}_4)_{0.5} \cdot 2\text{H}_2\text{O}$ (PO4_SO4) and calcium sulfate dihydrate $\text{CaSO}_4 \cdot 2\text{H}_2\text{O}$ (SO4). The phase composition of PO4 powder after disaggregation in acetone included sodium chloride NaCl and monetite CaHPO_4 , which was formed from metastable brushite $\text{CaHPO}_4 \cdot 2\text{H}_2\text{O}$ according to Reaction (4).



The compositions of the synthesized powders after disaggregation were estimated using Match! software (Table 3).

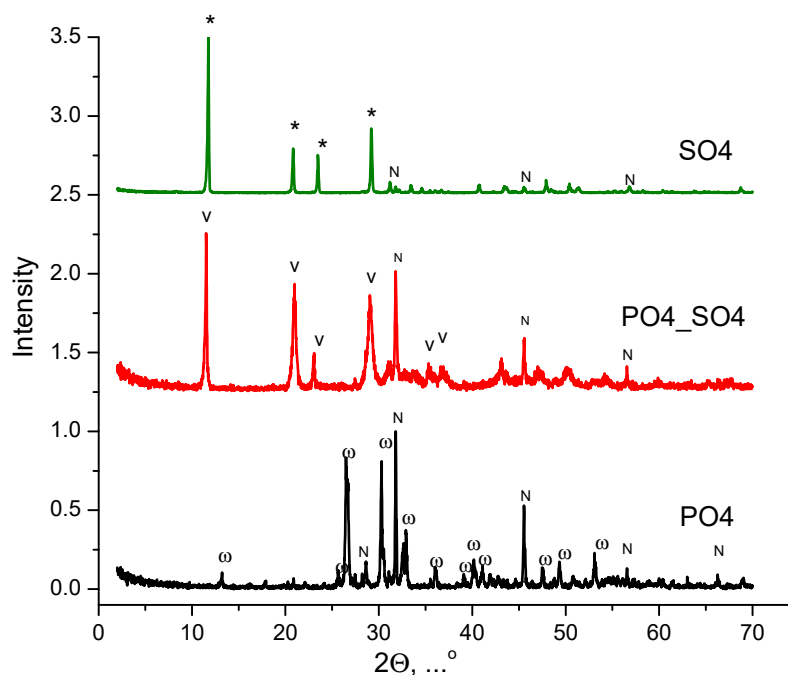


Figure 3. XRD data of powders synthesized from aqueous solution of calcium chloride CaCl_2 and sodium sulfate Na_2SO_4 (green line); from aqueous solution of calcium chloride CaCl_2 and sodium hydrophosphate Na_2HPO_4 (black line); and from aqueous solution of calcium chloride CaCl_2 and mixed-anionic solution $\text{Na}_2\text{HPO}_4/\text{Na}_2\text{SO}_4$ (red line) after disaggregation in acetone: *— $\text{CaSO}_4 \cdot 2\text{H}_2\text{O}$ (card PDF 21-816); N— NaCl (card PDF 5-628); v— $\text{Ca}(\text{HPO}_4)_x(\text{SO}_4)_{1-x} \cdot 2\text{H}_2\text{O}$ (PDF card 46-657); $\text{Ca}(\text{HPO}_4)_{0.5}(\text{SO}_4)_{0.5} \cdot 2\text{H}_2\text{O}$ (Match card 96-900-0654); ω — CaHPO_4 (карточка PDF 9-80).

Table 3. Composition of synthesized powders after disaggregation, wt. %.

Sample	Powder Composition			
	CaHPO_4	$\text{CaSO}_4 \cdot 2\text{H}_2\text{O}$	$\text{Ca}(\text{HPO}_4)_{0.5}(\text{SO}_4)_{0.5} \cdot 2\text{H}_2\text{O}$	NaCl
PO4	83.4	-	-	16.6
PO4_SO4	-	-	72.5	27.5
SO4	-	98.1	-	1.9

On the basis of these data, the quantity of sodium chloride NaCl captured as by-product in the synthesized powders after disaggregation can be estimated to be noticeable for the PO4 and PO4_SO4 samples.

In Figure 4, the FTIR spectra of the samples after disaggregation are presented. In the spectrum of the PO4 sample, the characteristic bands of phosphate groups are present. The bands at 1126 , 1063 , 995 , 891 cm^{-1} can be attributed to valence vibrations, while the band at 554 cm^{-1} can be attributed to deformation vibrations of P-O bands in the phosphate group. In the spectrum of the SO4 sample, the bands of sulphate groups can be observed: the peak at 1106 cm^{-1} corresponds to valence vibrations, while the peaks at 667 and 596 cm^{-1} correspond to deformation vibrations. Additionally, in the spectrum of the SO4 sample, the bands of OH bonds can be observed (3526 and 3394 cm^{-1} —valence vibrations; 1686 and 1622 cm^{-1} —deformation vibrations). The spectrum of the PO4_SO4 sample contains the bands of both sulphate and phosphate groups. The bands are slightly shifted, indicating the formation of an ardalite structure, as observed in the XRD patterns (Figures 1 and 3). The FTIR spectra of the powders prepared in this work have some features in common with those of powders prepared in previous work [63].

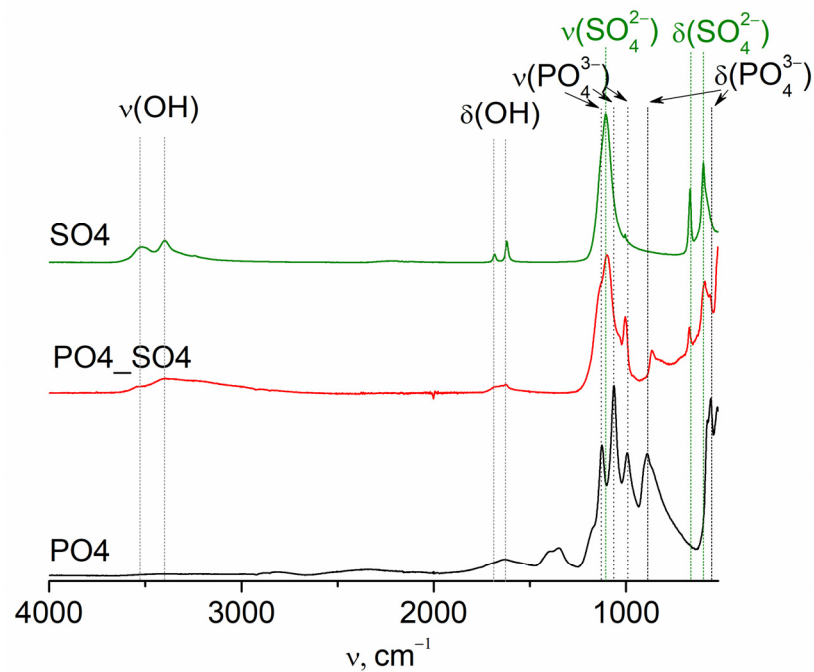


Figure 4. FTIR spectra of the samples after disaggregation in acetone.

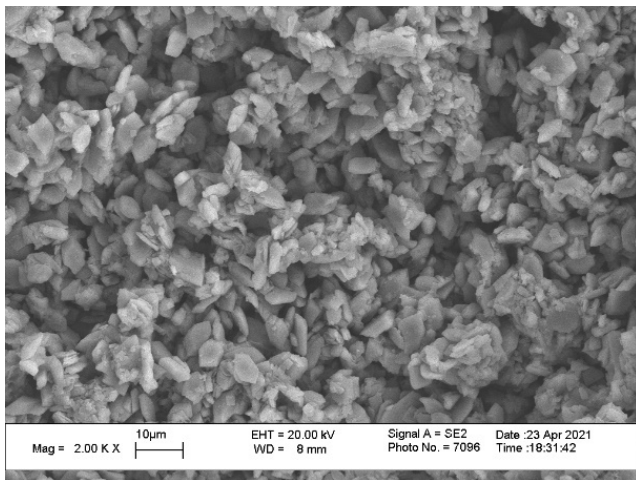
Figure 5 shows micrographs of powders after synthesis and disaggregation. Particles of PO4 powder after synthesis ($\text{CaHPO}_4 \cdot 2\text{H}_2\text{O}$ according to XRD data, Figure 1) had a plate-like morphology and dimensions of 1–5 μm . After disaggregation, particles of PO4 (CaHPO_4) powder had a plate-like morphology and dimensions not bigger than 1 μm . The mechanical impact of grinding media and the dehydration process are probable reasons for the decrease in particle size. Powder SO4 ($\text{CaSO}_4 \cdot 2\text{H}_2\text{O}$, according to the XRD data, Figure 1) after synthesis consisted of plate-like (4–8 μm) and column-like particles (2–8 μm). After disaggregation, fractions of smaller plate-like (4–8 μm) and columnar-like (2–8 μm) particles increased in SO4 powder. The PO4_SO4 powder consisted of aggregates (2–4 μm) of equiaxed particles with dimensions 100–300 nm. After treatment in acetone medium using a planetary mill, particle aggregates mainly had dimensions of about 2 μm . After disaggregation, the dimensions of the particles and aggregates were smaller in all powders under investigation. Particle morphology and the size of powders under investigation (Figure 5) correlated well with the estimated by-product quantities (Table 1). The larger the particle size and the lower the specific surface area, the lower the quantity of captured by-product. Similar correlations have been observed in previous work [51].

The bulk density of synthesized powders and powders after disaggregation, as well as the density of pre-ceramic samples after pressing at 100 MPa, are presented in Table 4.

Table 4. Bulk density of powders after synthesis and disaggregation in acetone, as well as the density of samples after pressing at 100 MPa (g/cm^3).

Sample	Powder after Synthesis	Powder after Disaggregation	Pre-Ceramic Sample after Pressing at 100 MPa	Densification, Degree
PO4	0.78	0.34	1.68	$1.68/0.34 = 4.9$
PO4_SO4	0.55	0.44	1.34	$1.34/0.44 = 3.0$
SO4	0.42	0.37	1.50	$1.50/0.37 = 4.1$

After synthesis

(a) PO₄ synth

After disaggregation

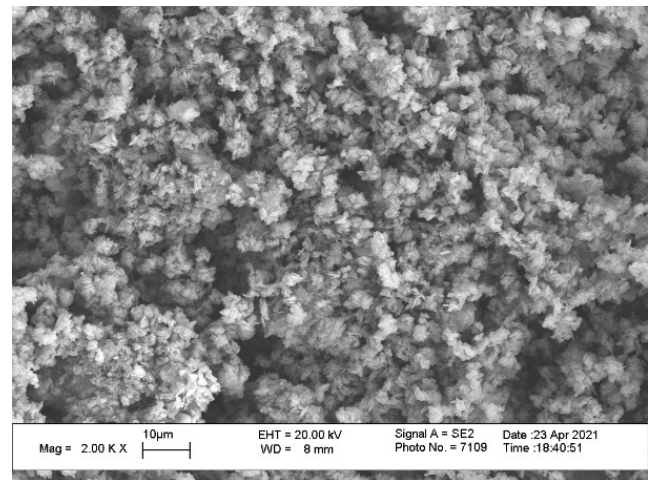
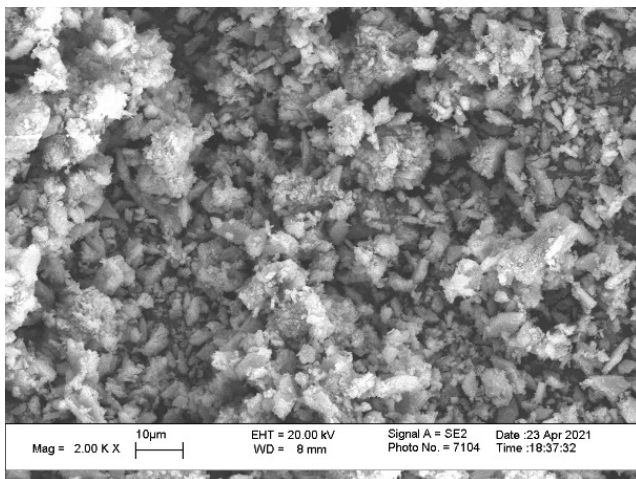
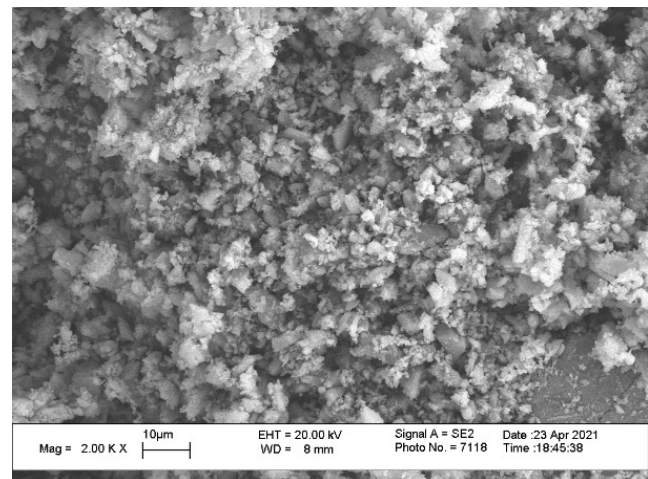
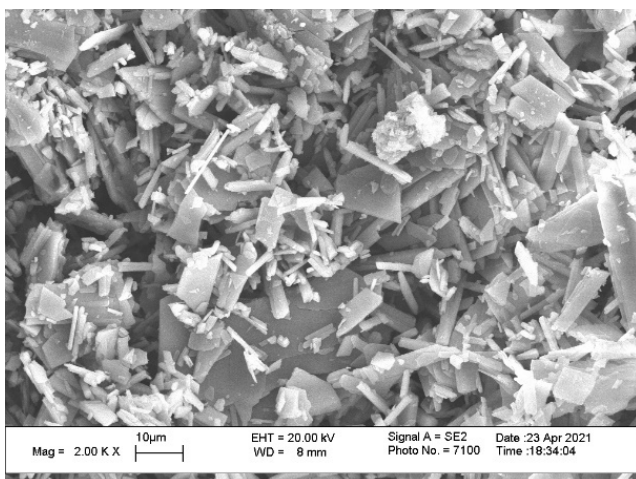
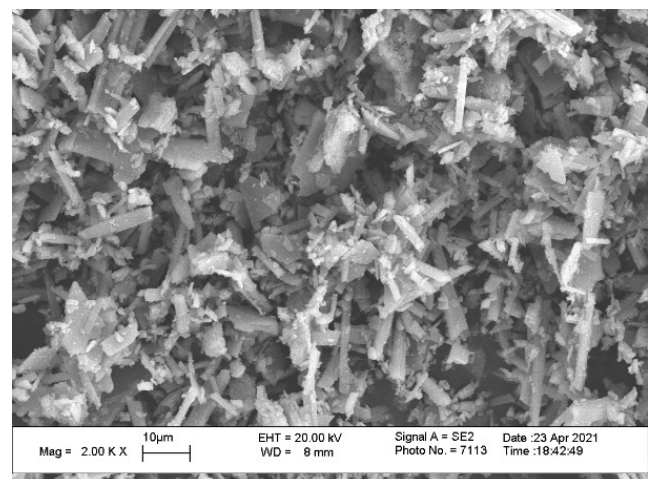
(b) PO₄ disaggr(c) SO₄_PO₄ synth(d) SO₄_PO₄ disaggr(e) SO₄ synth(f) SO₄ disaggr

Figure 5. SEM images of powders after synthesis (left column, (a,c,e)) and after disaggregation in acetone (right column (b,d,f)).

The micrographs (Figure 4) and the bulk density of the powders (Table 4) indicate that disaggregation in acetone medium leads to a decrease in particle size and to a decrease in

the bulk density of the powders. PO4 powder demonstrated the best tendency towards densification. After pressing at 100 MPa, the density of the PO4 pre-ceramic powder samples increased by 4.9 times compared to the bulk density of the powders after disaggregation, which was probably due to the plate-like morphology of particles. The density of the SO4 pre-ceramic powder samples was 4.1 times greater than the bulk density of the powder after disaggregation. The PO4_SO4 powder demonstrated the lowest tendency towards densification, with the bulk density of the powder being only 3 times lower than the density of the pre-ceramic powder samples.

Thermogravimetry (TG) curves for the synthesized powders are shown in Figure 6. Differential scanning calorimetry (DSC) curves and MS curves of evolving gases with $m/Z = 18$ (H_2O) and $m/Z = 64$ (SO_2) for the synthesized powders are shown in Figure 7.

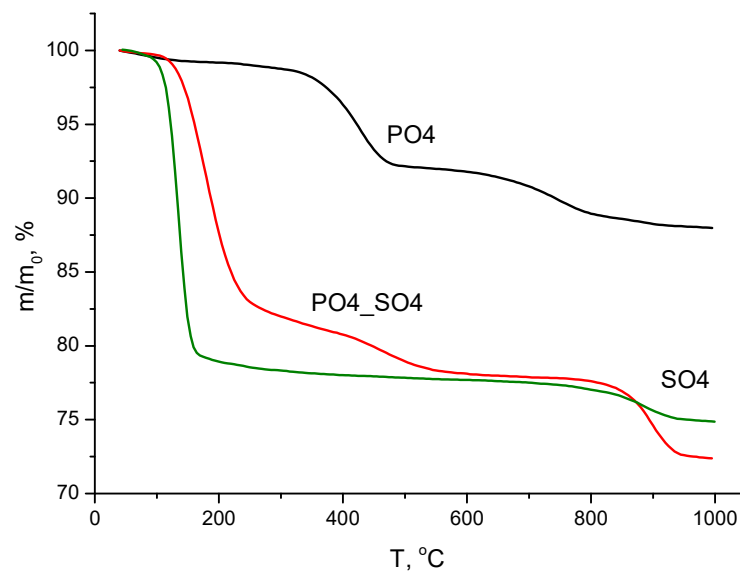
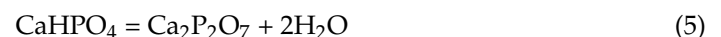
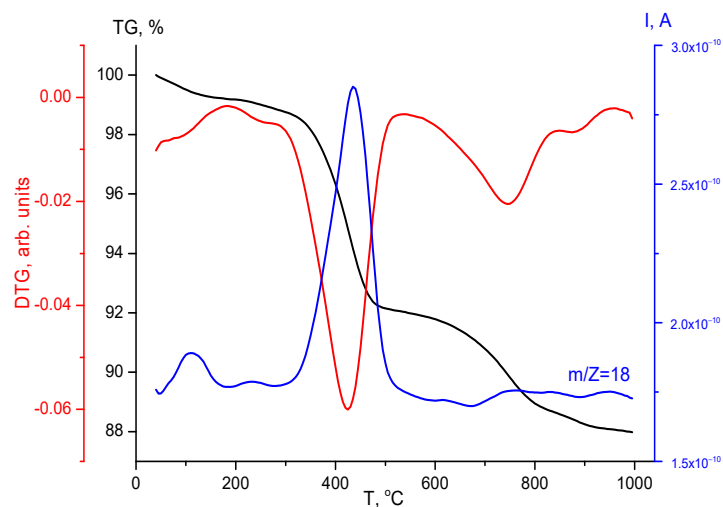


Figure 6. TG curves of powders synthesized from aqueous solution of calcium chloride $CaCl_2$ and sodium sulfate Na_2SO_4 (green line); from aqueous solution of calcium chloride $CaCl_2$ and sodium hydrophosphate Na_2HPO_4 (black line); and from aqueous solution of calcium chloride $CaCl_2$ and mixed-anionic solution Na_2HPO_4/Na_2SO_4 (red line) after disaggregation in acetone.

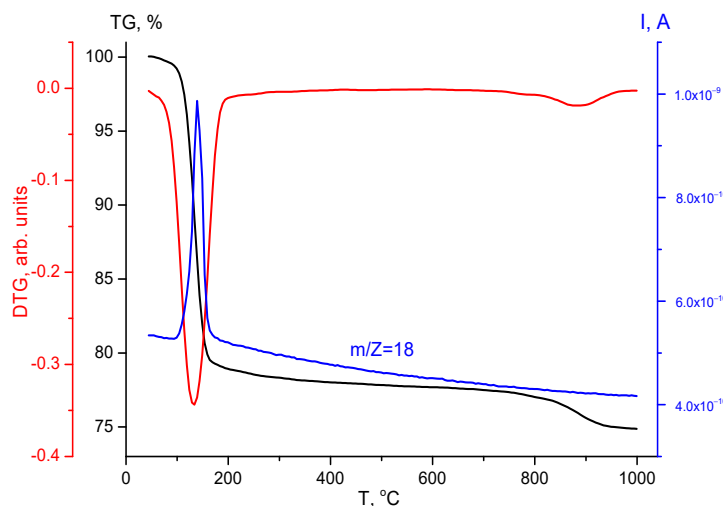
The total mass loss of the PO4 powder when heated to 1000 °C was 12.1% (Figures 6 and 7a). Physically bonded water (about 0.8%) leaves the sample in the interval 40–184 °C, with a maximum at 100 °C, according to MS curve for $m/Z = 18$ (Figure 7a). Then, a slight additional mass loss (about 0.4%) occurs in the interval 184–283 °C. Then, there are two noticeable steps on the mass loss curve of the PO4 powder. The first noticeable step, with a mass loss 6.7% in the interval 283–525 °C, with a maximum at 424 °C, on the DTG curve, corresponding to the maximum at 434 °C in the interval 287–570 °C on the MS curve for $m/Z = 18$, can be attributed to the thermal decomposition of monetite (Reaction (5)).



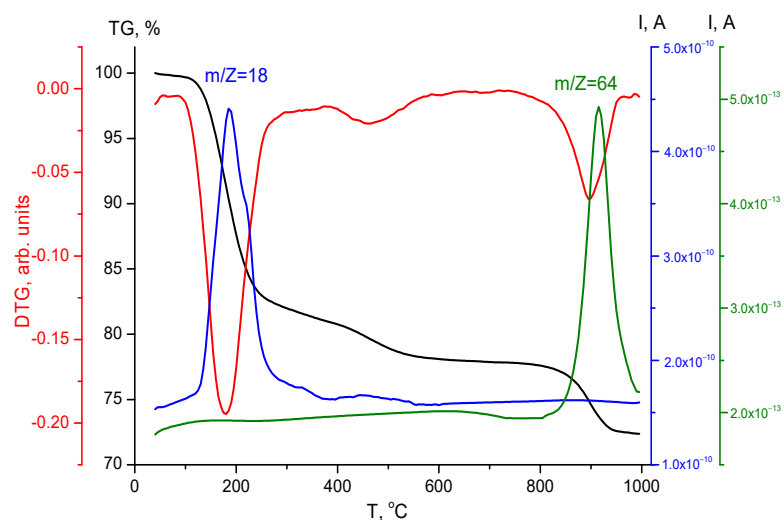
The second noticeable step, with mass loss 3.5% during the interval 525–845 °C with maximum at 745 °C on the DTG curve, showed no agreement with the MS curve for $m/Z = 18$. A slight peak (880 °C) was present in the interval 845–960 °C on the DTG curve, corresponding to a mass loss of 0.6%.



(a) PO₄



(b) SO₄



(c) PO₄_SO₄

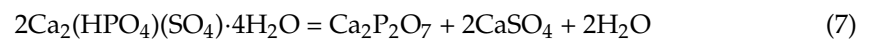
Figure 7. DTG and selected mass-spectra of powders synthesized from aqueous solution of calcium chloride CaCl₂ and sodium hydrophosphate Na₂HPO₄ (a); from aqueous solution of calcium chloride CaCl₂ and sodium sulfate Na₂SO₄ (b); and from aqueous solution of calcium chloride CaCl₂ and mixed-anionic solution Na₂HPO₄/Na₂SO₄ (c) after disaggregation in acetone.

The total mass loss of the SO₄ powder when heated to 1000 °C was 25.1% (Figures 6 and 7b). Sharp peaks are present in both the interval 40–190, with a maximum at 134 °C on the DTG curve, and in the interval 40–204 °C, at 140 °C on the MS (m/Z = 18) curve. This mass loss (21.1%) and the evolution of water reflect the process of thermal decomposition of calcium sulfate dihydrate according to Reaction (6). The calculated mass loss (21%) of this reaction is in perfect agreement with the thermal analysis data. The lower heating rate gives the opportunity to distinguish two mass loss steps during dehydration, with the formation of calcium sulfate hemihydrate and then calcium sulfate anhydrite [73].

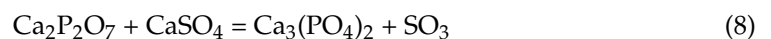


A slight mass decrease (1.9%) is observed in SO₄ powder in the interval 204–808 °C. In addition, mass loss (2.1%) occurs in the interval 808–965 °C, with a maximum at 886 °C. No ion current was detected in this interval for m/Z = 64 (SO₂) or m/Z = 18 (H₂O).

The total mass loss of the PO₄_SO₄ powder when heated to 1000 °C was 27.5% (Figures 6 and 7c). It should be noted that the character of the TG curve is very much similar to that of ardealite, investigated previously [74]. Several segments can be highlighted on the TG, DTG and MS graphs. Mass loss (18%) in the interval 80–300 °C, with a maximum at 180 °C on the DTG curve, is in agreement with the interval 110–330 and maximum at 187 °C on MS (m/Z = 18). A slight mass decrease (~1%) occurs in the interval 300–380 °C without noticeable signs on the DTG curve and some hint of the evolution of water on MS for m/Z = 18. The evolution of water is probably the reason for the mass loss (3%) in the interval 380–590 °C, with a maximum at 460 °C detected on the DTG curve. The mass loss (22%) up to 590 °C for ardealite powder synthesized in this work is in good correlation with thermal analysis data presented for ardealite powder in [53]. The decomposition of ardealite during heating to 590 °C is reflected by formal Reaction (7).



In the interval 590–750 °C, no mass loss was detected. Then, in the interval 750–975 °C, with a maximum at 898 °C, on the DTG curve, mass loss of 5.5% was detected. According to the MS curve, this mass loss was due to the evolution of SO₃ (SO₂ can be detected). The presence of calcium pyrophosphate Ca₂P₂O₇ and calcium sulfate anhydrite CaSO₄ makes Reaction (8) possible.



According to the literature data, the thermal stability of calcium sulfate anhydrite CaSO₄ is possible in the temperature range of 1000–1400 °C [75,76]. In the production of ceramics containing calcium sulfate anhydrite CaSO₄ and tricalcium phosphate Ca₃(PO₄)₂, the firing temperature, after which the phase composition did not include calcium oxide toxic to the body, is indicated as 1050 °C [17]. The presence of other salts or phases reduces the thermal stability of calcium sulfate anhydrite CaSO₄ [77].

Table 5 presents a summary of the XRD data for powders after synthesis and disaggregation, as well as for ceramics based on them after firing at various temperatures (800, 900, 1000, 1100 °C). XRD data of ceramic samples after firing at 900 °C is presented in Figure 8.

Table 5. Phase composition of samples at various stages of powder preparation and ceramics production.

Stage	Samples		
	PO4	PO4_SO4	SO4
Powders			
Synthesis	CaHPO ₄ ·2H ₂ O CaHPO ₄ NaCl	Ca(HPO ₄) _x (SO ₄) _{1-x} ·2H ₂ O (Ca(HPO ₄) _{0.5} (SO ₄) _{0.5} ·2H ₂ O) NaCl	CaSO ₄ ·2H ₂ O NaCl
Disaggregation	CaHPO ₄ NaCl	Ca(HPO ₄) _x (SO ₄) _{1-x} ·2H ₂ O (Ca(HPO ₄) _{0.5} (SO ₄) _{0.5} ·2H ₂ O) NaCl	CaSO ₄ ·2H ₂ O NaCl
Ceramics			
Firing, 800 °C	β-Ca ₂ P ₂ O ₇ Ca ₅ (PO ₄) ₃ Cl amorphous phase	β-Ca ₂ P ₂ O ₇ CaSO ₄ Ca ₅ (PO ₄) ₃ Cl β-Ca ₂ P ₂ O ₇	CaSO ₄
Firing, 900 °C	β-Ca ₂ P ₂ O ₇ Ca ₅ (PO ₄) ₃ Cl amorphous phase	CaSO ₄ Ca ₅ (PO ₄) ₃ Cl amorphous phase	CaSO ₄ (Na _{0.8} Ca _{0.1}) ₂ SO ₄
Firing, 1000 °C	β-Ca ₂ P ₂ O ₇ Ca ₅ (PO ₄) ₃ Cl amorphous phase	CaSO ₄ Ca ₅ (PO ₄) ₃ Cl Ca ₃ (PO ₄) ₂ /Ca ₁₀ Na(PO ₄) ₇ amorphous phase	CaSO ₄ (Na _{0.8} Ca _{0.1}) ₂ SO ₄
Firing, 1100 °C	Ca ₅ (PO ₄) ₃ Cl, amorphous phase	CaSO ₄ Ca ₅ (PO ₄) ₃ Cl amorphous phase	CaSO ₄ (Na _{0.8} Ca _{0.1}) ₂ SO ₄ amorphous phase

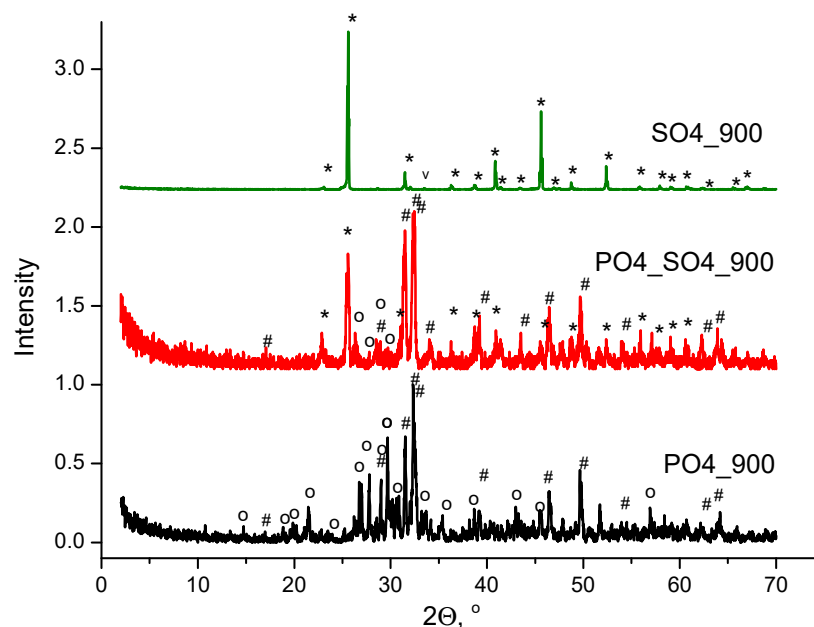


Figure 8. XRD data of ceramic samples based on powders synthesized from aqueous solution of calcium chloride CaCl₂ and sodium sulfate Na₂SO₄ (green line); based on aqueous solutions of calcium chloride CaCl₂ and sodium hydrophosphate Na₂HPO₄ (black line); and based on aqueous solutions of calcium chloride CaCl₂ and mixed-anionic solution Na₂HPO₄/Na₂SO₄ (red line) after firing at 900 °C: *—CaSO₄ (card PDF 37-1496); v—(Na_{0.8}Ca_{0.1})₂SO₄ (card PDF 29-1126); #—Ca₅(PO₄)₃Cl (card PDF 73-1728); o—β-Ca₂P₂O₇ (карточка PDF 9-346).

Phase composition of ceramic samples SO4 after firing at 800 °C included only the phase of calcium sulfate anhydrite CaSO₄, which formed from calcium sulfate dihydrate CaSO₄·2H₂O. The phase composition of SO4 ceramic samples after firing at 900, 1000 and 1100 °C included a barely detectable phase of double sulfate (Na_{0.8}Ca_{0.1})₂SO₄. The formation of this phase is possible in presence of sodium salts. The absence of any noticeable traces of NaCl according XRD data in the phase composition of these ceramic samples can be explained with possibility of NaCl melt (T_{melt} of NaCl—801 °C) transferred to the gaseous phase [58].

Phase composition of PO4 ceramic samples after firing at 800, 900 and 1000 °C included chlorapatite Ca₅(PO₄)₃Cl and β-calcium pyrophosphate β-Ca₂P₂O₇. β-Calcium pyrophosphate β-Ca₂P₂O₇ formed from monetite CaHPO₄. Formation of chlorapatite Ca₅(PO₄)₃Cl became possible due to the presence of sodium chloride NaCl. Molar ratio in starting calcium phosphate (monetite CaHPO₄—precursor of Ca₂P₂O₇) Ca/P = 1. Molar ratio in chlorapatite Ca₅(PO₄)₃Cl formed during firing Ca/P = 1.67. This fact makes it possible to suppose the rearrangement of Ca²⁺-cations and phosphate anions between crystal phase and melt. This rearrangement can be described by formal Reaction (9).



Polyphosphates, especially of alkali metals (Na or K), can be used as a sintering additive, promoting liquid phase sintering and reducing the firing temperature [78,79]. Two eutectic points are in the quasi-binary system NaPO₃-Ca(PO₃)₂: 625 °C and 721 °C. This fact can explain the presence of melt or quasi-amorphous phase in the PO4 ceramic sample already after firing at 800 °C. XRD data presented in Figure 8 confirms the presence of amorphous or quasi-amorphous phase, which presumably belongs to the system Na₂O-CaO-P₂O₅ or probably to the system Na₂O-CaO-P₂O₅-NaCl. After firing at 1100 °C, the PO4 ceramic sample went through melting and crystallization. The melt formed interacted with Al₂O₃ crucible. So phase composition of the ceramic sample ruins included Ca₅(PO₄)₃Cl and Ca₉Al(PO₄)₇. The second noticeable step, with a mass loss of 3.5% in the PO4 sample in the interval 525–845 °C with a maximum at 745 °C on the DTG curve has not yet been explained. Evacuation of low-temperature phosphate melt due to the high pressure above could potentially be a reason.

The phase composition of ceramic samples PO4_SO4 after firing at 800 and 900 °C included CaSO₄, Ca₅(PO₄)₃Cl and β-Ca₂P₂O₇. After firing at 1000 °C it included CaSO₄, Ca₅(PO₄)₃Cl and Ca₃(PO₄)₂ or Ca₁₀Na(PO₄)₇ with similar reflexes. After firing 1100 °C phase composition of ceramic samples PO4_SO4 included CaSO₄ and Ca₅(PO₄)₃Cl. Ceramic samples PO4_SO4 after firing at all temperatures except crystalline phases mentioned above included some quantity of amorphous or quasi-amorphous phase. Ardealite can be treated as a highly homogenous precursor of both calcium pyrophosphate and calcium sulfate anhydrite. The presence of sodium chloride and calcium phosphate was the reason for chlorapatite Ca₅(PO₄)₃Cl formation. Therefore, the formation of melt in the samples is also possible for the same reasons as in PO4 ceramic samples.

Ceramic samples had the highest density after firing at 900 °C (Figure 9): PO4—2.39 g/cm³, PO4_SO4—2.23 g/cm³ and SO4—1.89 g/cm³. The sample based on PO4_SO4 powder had a maximum linear shrinkage after firing at 900 °C—23% (Figure 10). The reduction in the density and the increase in the linear dimensions of the samples after firing at 1000 °C relative to the densities and dimensions after firing at 900 °C can be explained by the evaporation of melts reaching or exceeding the melt temperature.

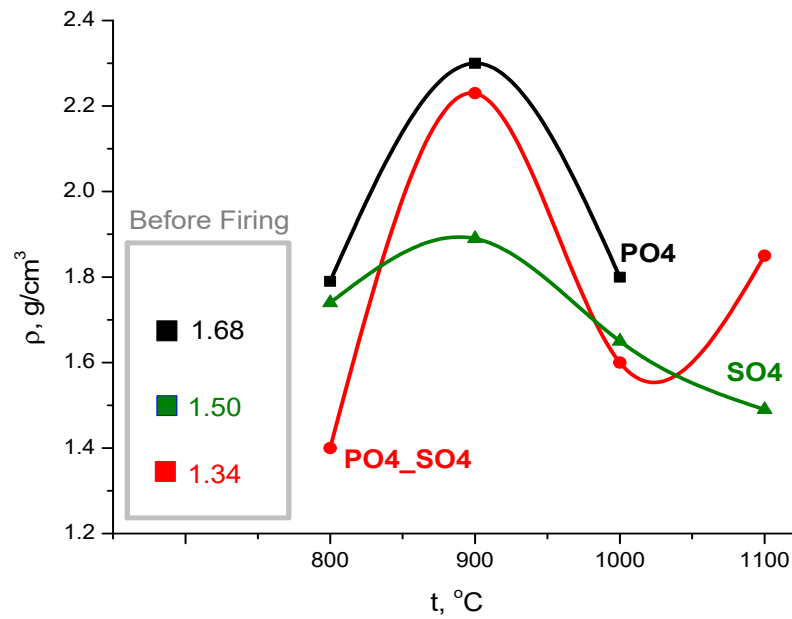


Figure 9. Temperature dependence of density of ceramic samples after firing.

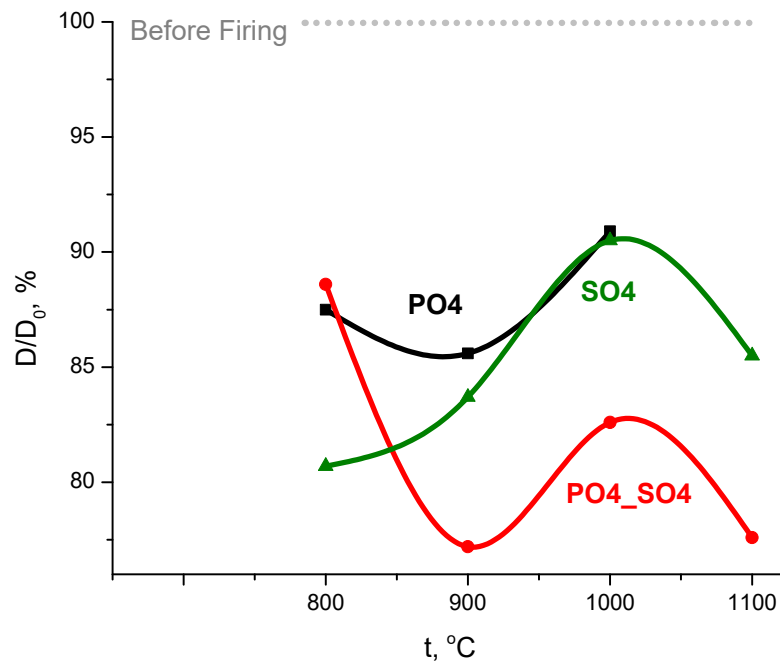


Figure 10. Temperature dependence of diameter of ceramic samples after firing.

Figure 11 shows micrographs of the cross-sections of polycrystalline ceramic samples after firing at 900 °C. The microstructure of the sample of PO4 ceramics consisted of small grains (~0.5 μm), with really big grains (~50 μm) and pores (8–50 μm) among them. The presence of melt in the sample during firing could provide conditions for local abnormal grain growth due to the processes of dissolution and crystallization. The microstructure of the sample of PO4_SO4 ceramics looks more uniform and consisted of small grains (1–5 μm) and pores (3–10 μm). It was difficult to estimate the dimensions of grains and pores between the grains in ceramic sample SO4. In the microstructure of ceramic sample SO4, intragrain pores with dimensions 3–10 μm can be seen. The presence of NaCl melt (T_{melt} of NaCl—801 °C) was probably the reason for the grain growth in SO4 ceramics before evacuation from the sample. In the absence of such an aggressive melt, ceramic

samples based on calcium sulfate anhydrite CaSO_4 consisted of small grains ranging in size from 0.2–1 μm after firing at 800 $^\circ\text{C}$ to 0.5–1 μm after firing at 1000 $^\circ\text{C}$ [23]. The microstructure of the ceramics prepared from SO_4 powder containing NaCl looks very similar to the microstructure of ceramics based on calcium sulfate anhydrite prepared with silicate glass as a sintering additive [26].

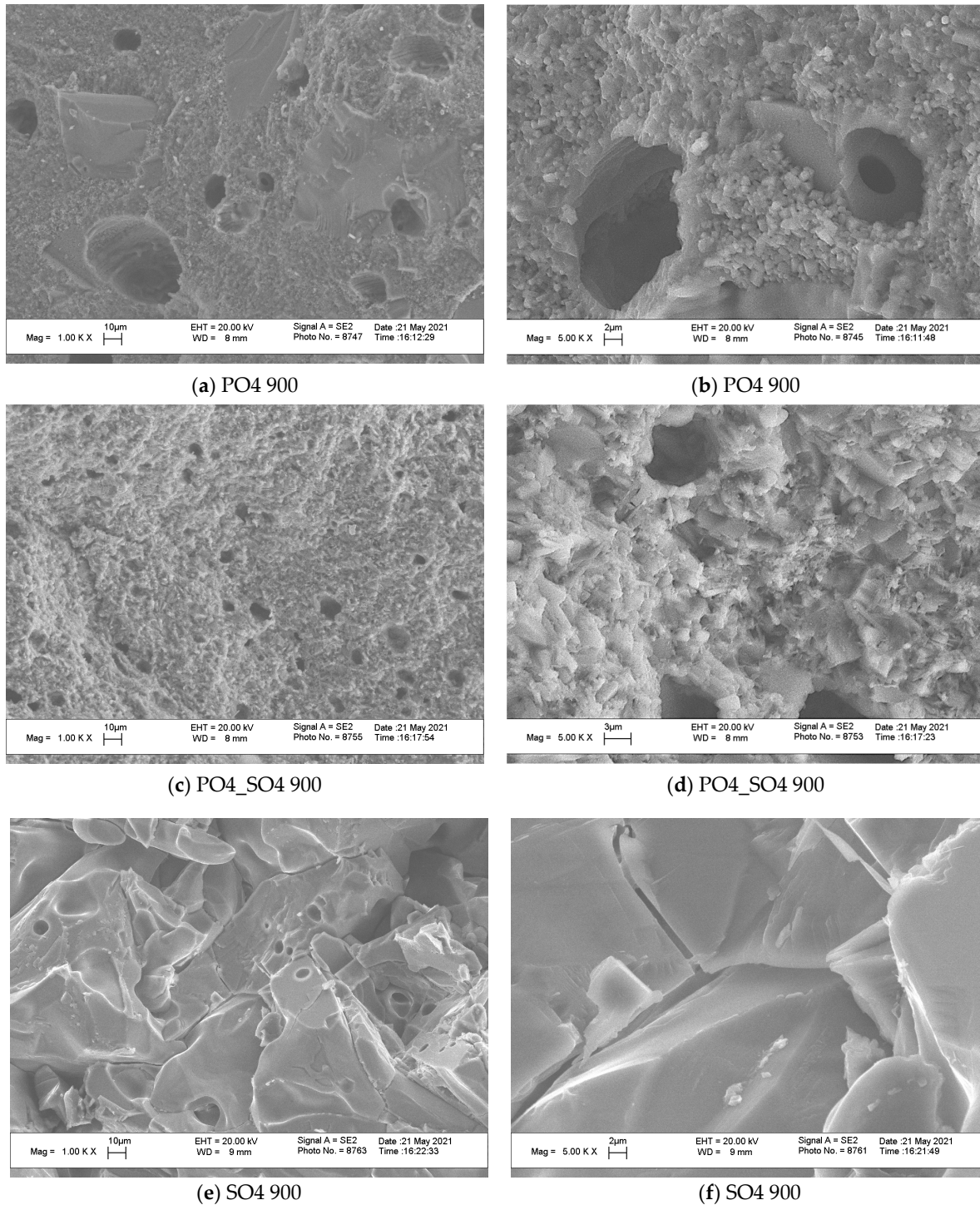


Figure 11. Micrographs of cross-sections of ceramic samples based on powders synthesized from calcium chloride CaCl_2 and sodium hydrophosphate Na_2HPO_4 solutions (a,b); based on calcium chloride CaCl_2 and mixed-anionic ($\text{Na}_2\text{HPO}_4/\text{Na}_2\text{SO}_4$) solutions (c,d); and based on calcium chloride CaCl_2 and sodium chloride Na_2SO_4 solutions (e,f), after firing at 900 $^\circ\text{C}$.

Figure 12 shows micrographs of the surfaces of ceramic samples based on a powder synthesized from calcium chloride CaCl_2 and a mixed-anionic solution of sodium hydrogen phosphate and sodium sulfate $\text{Na}_2\text{HPO}_4/\text{Na}_2\text{SO}_4$ after firing at different temperatures in interval 800–1000 °C.

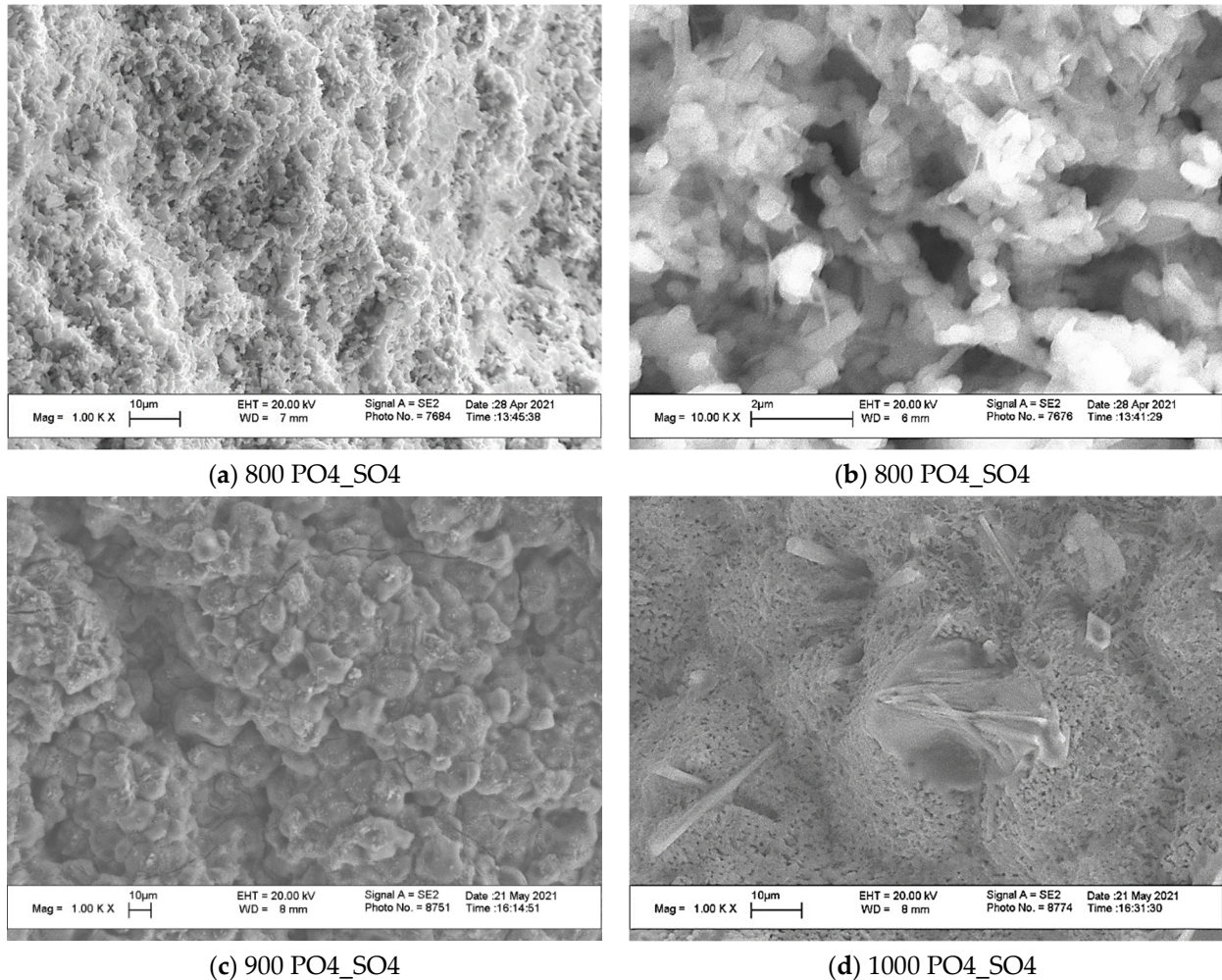


Figure 12. Micrographs of the surface of ceramic samples based on a powder synthesized from calcium chloride CaCl_2 and a mixed-anionic solution of sodium hydrophosphate and sodium sulfate $\text{Na}_2\text{HPO}_4/\text{Na}_2\text{SO}_4$ after firing at 800 (a,b), 900 (c), 1000 (d).

The surfaces of the PO4_SO4 ceramic samples look very different after firing at different temperatures. It can be seen that elongated crystals with the smallest dimension not bigger than 100 nm have grown on the surfaces of the grains, supposedly via gas phase mechanism after firing at 800 °C (Figure 12a,b). This phenomenon could occur due to the possible presence of NaCl melt or melt of more complicated composition presumably in the system $\text{Na}_2\text{O}-\text{CaO}-\text{P}_2\text{O}_5-\text{NaCl}$ or even in the system $\text{Na}_2\text{O}-\text{CaO}-\text{P}_2\text{O}_5-\text{SO}_3-\text{NaCl}$ with high pressure of melt vapor. The images of the PO4_SO4 ceramic sample cross-section (Figure 11b) and surface (Figure 12c) after firing at 900 °C are in agreement with data on density (Figure 9) and liner shrinkage (Figure 10). The surface of the ceramic sample PO4_SO4 after firing at 1000 °C (Figure 12d) looks porous with very small (1–2 µm) pores as after the escape of boiling melt, which was certainly the cause of the formation of this original porosity. Some large elongated crystals with dimension not less than 30 µm can be observed, growing from the regions with a porous structure.

4. Conclusions

Powder PO4_SO4 of ardealite $\text{Ca}(\text{HPO}_4)_x(\text{SO}_4)_{1-x} \cdot 2\text{H}_2\text{O}$ (or $\text{Ca}(\text{HPO}_4)_{0.5}(\text{SO}_4)_{0.5} \cdot 2\text{H}_2\text{O}$) containing sodium chloride NaCl as a reaction by-product was synthesized by means of precipitation from water solution of calcium chloride CaCl_2 and mixed-anionic water solution containing simultaneously the hydrogen phosphate anion HPO_4^{2-} (from NaHPO_4) and sulfate anion SO_4^{2-} (from Na_2SO_4). To the best of our knowledge, powder of ardealite was used for production of ceramics here for the first time. Ardealite as precursor due to crystalline structure can ensure high homogeneity of distribution of phases in ceramics.

For comparison, powders of brushite $\text{CaHPO}_4 \cdot 2\text{H}_2\text{O}$ (PO4) and calcium sulfate dihydrate $\text{CaSO}_4 \cdot 2\text{H}_2\text{O}$ (SO4) containing sodium chloride NaCl_2 were synthesized from water solutions of two pairs of salts: CaCl_2 and NaHPO_4 ; and CaCl_2 and Na_2SO_4 . Mother liquors after separation of precipitates contained NaCl (for PO4 synthesis), and $\text{NaCl} + \text{CaSO}_4 \cdot 2\text{H}_2\text{O}$ for the rest two (PO4_SO4 and SO4) syntheses. Preservation of sodium chloride NaCl as a reaction by-product in all synthesized powders was also used as an approach to reach appropriate homogeneity of distribution of components in starting powders.

Phase composition of SO4 ceramics based on powder of calcium sulfate dihydrate $\text{CaSO}_4 \cdot 2\text{H}_2\text{O}$ ($\text{NaCl}/\text{CaSO}_4 \cdot 2\text{H}_2\text{O}$) after firing at 800–1100 °C included calcium sulfate anhydrite CaSO_4 as the dominant phase and $(\text{Na}_{0.8}\text{Ca}_{0.1})_2\text{SO}_4$ as slightly noticeable. Microstructure of SO4 ceramics formed under assistance of melt including NaCl presented during firing in the sample and then escaped.

The phase composition of PO4 ceramics based on powder of brushite $\text{CaHPO}_4 \cdot 2\text{H}_2\text{O}$ (NaCl) after firing at 800–900 °C included $\beta\text{-Ca}_2\text{P}_2\text{O}_7$, $\text{Ca}_5(\text{PO}_4)_3\text{Cl}$, and, according to XRD data, a noticeable quantity of quasi-amorphous phase. Some regions of this PO4 ceramic sample after firing at 900 °C had a uniform structure with grain size about $\sim 0.5 \mu\text{m}$. Among them really big grains ($\sim 50 \mu\text{m}$) and pores (8–50 μm) presented.

The phase composition of ceramics based on powder of ardealite $\text{Ca}(\text{HPO}_4)_x(\text{SO}_4)_{1-x} \cdot 2\text{H}_2\text{O}$ ($\text{NaCl}/\text{CaSO}_4 \cdot 2\text{H}_2\text{O}$) after firing at 800 °C included $\beta\text{-Ca}_2\text{P}_2\text{O}_7$, CaSO_4 , $\text{Ca}_5(\text{PO}_4)_3\text{Cl}$. After firing at 900 °C, according XRD data, a noticeable quantity of quasi-amorphous phase was additionally detected. After firing at 1000 °C, CaSO_4 , $\text{Ca}_5(\text{PO}_4)_3\text{Cl}$, $\text{Ca}_3(\text{PO}_4)_2/\text{Ca}_{10}\text{Na}(\text{PO}_4)_7$ and amorphous phases were detected. In addition, after firing at 1100 phase composition included CaSO_4 , $\text{Ca}_5(\text{PO}_4)_3\text{Cl}$ and amorphous phases. The microstructure of the sample of PO4_SO4 ceramics looks more uniform and consisted of small grains (1–5 μm) and pores (3–10 μm).

The presence of sodium chloride NaCl in powders under investigation was responsible for low-temperature melt formation and for hetero phase interaction of components with formation of chlorapatite $\text{Ca}_5(\text{PO}_4)_3\text{Cl}$ and, as can be assumed, $\text{Ca}_{10}\text{Na}(\text{PO}_4)_7$. Presumably, melt with high content of P_2O_5 could form in the system $\text{Na}_2\text{O}-\text{CaO}-\text{P}_2\text{O}_5-\text{NaCl}$ in ceramic samples of PO4 and PO4_SO4. Such melt vapor at high pressure could be the reason for the loss of mass in these samples and the decrease in the content of amorphous phase in the phase composition of ceramics with increasing firing temperature.

Crystalline phases detected by means of XRD are known to be biocompatible, but the composition of amorphous phase of ceramics remains unknown. Therefore, additional investigations are necessary to confirm the possibility to use prepared ceramics in medicine for bone defect treatment.

Author Contributions: Conceptualization, T.V.S.; methodology, T.V.S.; validation, T.V.S., T.B.S., I.V.K., A.V.K.; investigation, T.V.S., A.S.K., T.B.S., Y.Y.F., I.V.K., A.V.K.; resources, T.B.S., Y.Y.F., I.V.K., A.V.K.; data curation, T.V.S., A.V.K.; writing—original draft preparation, T.V.S. and A.S.K.; writing—review and editing, T.V.S.; visualization, T.V.S., A.S.K., T.B.S., Y.Y.F., I.V.K., A.V.K.; supervision, T.V.S.; project administration, T.V.S.; funding acquisition, T.V.S. All authors have read and agreed to the published version of the manuscript.

Funding: This work was carried out with financial support from the Russian Foundation for Basic Research (RFBR) (grant no. 20-03-00550).

Institutional Review Board Statement: Not applicable.

Informed Consent Statement: Not applicable.

Data Availability Statement: Not applicable.

Acknowledgments: This research was carried out using the equipment of the MSU Shared Research Equipment Center “Technologies for obtaining new nanostructured materials and their complex study”, and purchased by MSU in the frame of the Equipment Renovation Program (National Project “Science”), and in the frame of the MSU Program of Development.

Conflicts of Interest: The authors declare no conflict of interest.

References

1. Navarro, M.; Michiardi, A.; Castan, O.; Planell, J.A. Biomaterials in orthopaedics. *J. R. Soc. Interface* **2008**, *5*, 1137–1158. [[CrossRef](#)]
2. Safronova, T.V. Inorganic materials for regenerative medicine. *Inorg. Mater.* **2021**, *57*, 443–474. [[CrossRef](#)]
3. Hou, X.; Zhang, L.; Zhou, Z.; Luo, X.; Wang, T.; Zhao, X.; Lu, B.; Chen, F.; Zheng, L. Calcium Phosphate-Based Biomaterials for Bone Repair. *J. Funct. Biomater.* **2022**, *13*, 187. [[CrossRef](#)]
4. Niu, Y.Q.; Liu, J.H.; Aymonier, C.; Fermani, S.; Kralj, D.; Falini, G.; Zhou, C.H. Calcium carbonate: Controlled synthesis, surface functionalization, and nanostructured materials. *Chem. Soc. Rev.* **2022**, *51*, 7883–7943. [[CrossRef](#)]
5. Combes, C.; Bareille, R.; Rey, C. Calcium carbonate–calcium phosphate mixed cement compositions for bone reconstruction. *J. Biomed. Mater. Res. A* **2006**, *79A*, 318–328. [[CrossRef](#)]
6. Yukna, R.A. Clinical evaluation of coralline calcium carbonate as a bone replacement graft material in human periodontal osseous defects. *J. Periodontol.* **1994**, *65*, 177–185. [[CrossRef](#)]
7. Youness, R.A.; Tag El-deen DM Taha, M.A. A Review on Calcium Silicate Ceramics: Properties, Limitations, and Solutions for Their Use in Biomedical Applications. *Silicon* **2022**. [[CrossRef](#)]
8. Almulhim, K.S.; Syed, M.R.; Alqahtani, N.; Alamoudi, M.; Khan, M.; Ahmed, S.Z.; Khan, A.S. Bioactive Inorganic Materials for Dental Applications: A Narrative Review. *Materials* **2022**, *15*, 6864. [[CrossRef](#)]
9. Ros-Tàrraga, P.; Mazón, P.; Meseguer-Olmo, L.; De Aza, P.N. Revising the subsystem Nurse’s a-phase-silicocarnotite within the system $\text{Ca}_3(\text{PO}_4)_2\text{--Ca}_2\text{SiO}_4$. *Materials* **2016**, *9*, 322. [[CrossRef](#)]
10. Wu, C.; Chang, J. A review of bioactive silicate ceramics. *Biomed. Mater.* **2013**, *8*, 032001. [[CrossRef](#)]
11. Kuo, S.-T.; Wu, H.-W.; Tuan, W.-H.; Tsai, Y.-Y.; Wang, S.-F.; Sakka, Y. Porous calcium sulfate ceramics with tunable degradation rate. *J. Mater. Sci. Mater. Med.* **2012**, *23*, 2437–2443. [[CrossRef](#)]
12. Ene, R.; Nica, M.; Ene, D.; Cursaru, A.; Cirstoiu, C. Review of calcium-sulphate-based ceramics and synthetic bone substitutes used for antibiotic delivery in PJI and osteomyelitis treatment. *EFORT Open Rev.* **2021**, *6*, 297–304. [[CrossRef](#)]
13. Yahav, A.; Kurtzman, G.M.; Katzap, M.; Dudek, D.; Baranes, D. Bone regeneration: Properties and clinical applications of biphasic calcium sulfate. *Dent. Clin.* **2020**, *64*, 453–472. [[CrossRef](#)]
14. Walsh, W.R.; Morberg, P.; Yu, Y.; Yang, J.L.; Haggard, W.; Sheath, P.C.; Bruce, W.J.M. Response of a calcium sulfate bone graft substitute in a confined cancellous defect. *Clin. Orthop. Relat. Res.* **2003**, *406*, 228–236. [[CrossRef](#)]
15. Medvecky, L.; Giretova, M.; Stulajterova, R.; Luptakova, L.; Sopcak, T. Tetracalcium Phosphate/Monetite/Calcium Sulfate Hemihydrate Biocement Powder Mixtures Prepared by the One-Step Synthesis for Preparation of Nanocrystalline Hydroxyapatite Biocement-Properties and In Vitro Evaluation. *Materials* **2021**, *14*, 2137. [[CrossRef](#)]
16. Yang, D.A.; Yang, Z.; Li, X.; Di, L.Z.; Zhao, H. A study of hydroxyapatite/calcium sulphate bioceramics. *Ceram. Int.* **2005**, *31*, 1021–1023. [[CrossRef](#)]
17. Yang, Z.; Yang, D.A.; Zhao, H. Degradation behavior of calcium sulfate/ β -tricalcium phosphate composites in Tris. *Key Eng. Mater.* **2007**, *336*, 1635–1637. [[CrossRef](#)]
18. Urban, R.M.; Turner, T.M.; Hall, D.J.; Inoue, N.; Gitelis, S. Increased bone formation using calcium sulfate-calcium phosphate composite graft. *Clin. Orthop. Relat. Res.* **2007**, *459*, 110–117. [[CrossRef](#)]
19. Guo, H.; Wei, J.; Liu, C.S. Development of a degradable cement of calcium phosphate and calcium sulfate composite for bone reconstruction. *Biomed. Mater.* **2006**, *1*, 193–197. [[CrossRef](#)]
20. Laskus, A.; Kolmas, J. Ionic Substitutions in Non-Apatitic Calcium Phosphates. *Int. J. Mol. Sci.* **2017**, *18*, 2542. [[CrossRef](#)]
21. Safronova, T.; Kiselev, A.; Selezneva, I.; Shatalova, T.; Lukina, Y.; Filippov, Y.; Toshev, O.; Tikhonova, S.; Antonova, O.; Knotko, A. Bioceramics Based on β -Calcium Pyrophosphate. *Materials* **2022**, *15*, 3105. [[CrossRef](#)]
22. Gbureck, U.; Hölzel, T.; Biermann, I.; Barralet, J.E.; Grover, L.M. Preparation of tricalcium phosphate/calcium pyrophosphate structures via rapid prototyping. *J. Mater. Sci. Mater. Med.* **2008**, *19*, 1559–1563. [[CrossRef](#)]
23. Safronova, T.V.; Belokozenko, M.A.; Yahyoev, S.O.; Shatalova, T.B.; Kazakova, G.K.; Peranidze, K.K.; Toshev, O.U.; Khasanova, S.S. Ceramics Based on $\text{CaSO}_4 \cdot 2\text{H}_2\text{O}$ Powder Synthesized from $\text{Ca}(\text{NO}_3)_2$ and $(\text{NH}_4)_2\text{SO}_4$. *Inorg. Mater.* **2021**, *57*, 867–873. [[CrossRef](#)]
24. Hsu, P.Y.; Chang, M.P.; Tuan, W.H.; Lai, P.L. Effect of physical and chemical characteristics on the washout resistance of calcium sulfate pellets. *Ceram. Int.* **2018**, *44*, 8934–8939. [[CrossRef](#)]
25. Chang, M.P.; Hsu, H.C.; Tuan, W.H.; Lai, P.L. A Feasibility Study Regarding the Potential Use of Silica-Doped Calcium Sulfate Anhydrite as a Bone Void Filler. *J. Med. Biol. Eng.* **2017**, *37*, 879–886. [[CrossRef](#)]

26. Chang, M.P.; Tsung, Y.C.; Hsu, H.C.; Tuan, W.H.; Lai, P.L. Addition of a small amount of glass to improve the degradation behavior of calcium sulfate bioceramic. *Ceram. Int.* **2015**, *41*, 1155–1162. [[CrossRef](#)]
27. Zhou, J.; Gao, C.; Feng, P.; Tao Xiao, T.; Shuai, C.; Peng, S. Calcium sulfate bone scaffolds with controllable porous structure by selective laser sintering. *J. Porous. Mater.* **2015**, *22*, 1171–1178. [[CrossRef](#)]
28. Zhou, J.; Yuan, F.; Peng, S.; Xie, H.; Wu, P.; Feng, P.; Gao, C.; Yang, Y.; Guo, W.; Lai, D.; et al. Tunable Degradation Rate and Favorable Bioactivity of Porous Calcium Sulfate Scaffolds by Introducing Nano-Hydroxyapatite. *Appl. Sci.* **2016**, *6*, 411. [[CrossRef](#)]
29. Tushima, T.; Hamai, R.; Tafu, M.; Takemura, Y.; Fujita, S.; Chohji, T.S.; Tanda, S.; Li Qin, G.W. Morphology control of brushite prepared by aqueous solution synthesis. *J. Asian Ceram. Soc.* **2014**, *2*, 52–56. [[CrossRef](#)]
30. Boanini, E.; Pagani, S.; Tschon, M.; Rubini, K.; Fini, M.; Bigi, A. Monetite vs. Brushite: Different Influences on Bone Cell Response Modulated by Strontium Functionalization. *J. Funct. Biomater.* **2022**, *13*, 65. [[CrossRef](#)]
31. Safronova, T.V.; Shatalova, T.B.; Tikhonova, S.A.; Filippov, Y.Y.; Krut'ko, V.K.; Musskaya, O.N.; Kononenko, N.E. Synthesis of Calcium Pyrophosphate Powders from Phosphoric Acid and Calcium Carbonate. *Inorg. Mater. Appl. Res.* **2021**, *12*, 986–992. [[CrossRef](#)]
32. Zhou, H.; Yang, L.; Gbureck, U.; Bhaduri, S.B.; Sikder, P. Monetite, an important calcium phosphate compound—Its synthesis, properties and applications in orthopedics. *Acta Biomater.* **2021**, *127*, 41–55. [[CrossRef](#)]
33. Safronova, T.V.; Sadilov, I.S.; Chaikun, K.V.; Shatalova, T.B.; Filippov, Y.Y. Synthesis of Monetite from Calcium Hydroxyapatite and Monocalcium Phosphate Monohydrate under Mechanical Activation Conditions. *Russ. J. Inorg. Chem.* **2019**, *64*, 1088–1094. [[CrossRef](#)]
34. Safronova, T.V.; Putlyaev, V.I.; Kurbatova, S.A.; Shatalova, T.B.; Larionov, D.S.; Kozlov, D.A.; Evdokimov, P.V. Properties of amorphous calcium pyrophosphate powder synthesized via ion exchange for the preparation of bioceramics. *Inorg. Mater.* **2015**, *51*, 1177–1184. [[CrossRef](#)]
35. Safronova, T.V.; Putlyaev, V.I.; Ivanov, V.K.; Knot'ko, A.V.; Shatalova, T.B. Powders mixtures based on ammonium pyrophosphate and calcium carbonate for preparation of biocompatible porous ceramic in the CaO–P₂O₅ system. *Refract. Ind. Ceram.* **2016**, *56*, 502–509. [[CrossRef](#)]
36. Toshev, O.; Safronova, T.; Kaimonov, M.; Shatalova, T.; Klimashina, E.; Lukina, Y.; Malyutin, K.; Sivkov, S. Biocompatibility of Ceramic Materials in Ca₂P₂O₇–Ca(PO₃)₂ System Obtained via Heat Treatment of Cement-Salt Stone. *Ceramics* **2022**, *5*, 516–532. [[CrossRef](#)]
37. Bolarinwa, A.; Gbureck, U.; Purnell, P.; Bold, M.; Grover, L.M. Cement casting of calcium pyrophosphate based bioceramics. *Adv. Appl. Ceram.* **2010**, *109*, 291–295. [[CrossRef](#)]
38. Safronova, T.V.; Korneichuk, S.A.; Shatalova, T.B.; Lukina Yu, S.; Sivkov, S.P.; Filippov, Y.Y.; Krut'ko, V.K.; Musskaya, O.N. Ca₂P₂O₇–Ca(PO₃)₂ Ceramic Obtained by Firing β-Tricalcium Phosphate and Monocalcium Phosphate Monohydrate Based Cement Stone. *Glass Ceram.* **2020**, *77*, 165–172. [[CrossRef](#)]
39. Asadi-Eydivand, M.; Solati-Hashjin, M.; Shafiei, S.S.; Mohammadi, S.; Hafezi, M.; Abu Osman, N.A. Structure, properties, and in vitro behavior of heat-treated calcium sulfate scaffolds fabricated by 3D printing. *PLoS ONE* **2016**, *11*, e0151216. [[CrossRef](#)]
40. Rahman, F. Calcium sulfate precipitation studies with scale inhibitors for reverse osmosis desalination. *Desalination* **2013**, *319*, 79–84. [[CrossRef](#)]
41. Combes, C.; Rey, C. Amorphous calcium phosphates: Synthesis, properties and uses in biomaterials. *Acta biomater.* **2010**, *6*, 3362–3378. [[CrossRef](#)]
42. Mosina, M.; Locs, J. Synthesis of Amorphous Calcium Phosphate: A Review. *Key Eng. Mater.* **2020**, *850*, 199–206. [[CrossRef](#)]
43. Kukueva, E.V.; Putlyaev, V.I.; Tikhonov, A.A.; Safronova, T.V. Octacalcium phosphate as a precursor for the fabrication of composite bioceramics. *Inorg. Mater.* **2017**, *53*, 212–219. [[CrossRef](#)]
44. Kukueva, E.V.; Putlyaev, V.I.; Safronova, T.V.; Tikhonov, A.A. Composite bioceramic based on octacalcium phosphate decomposition products. *Glass Ceram.* **2017**, *74*, 67–72. [[CrossRef](#)]
45. Safronova, T.V.; Putlyaev, V.I.; Filippov, Y.; Knot'ko, A.V.; Klimashina, E.S.; Peranidze, K.K.; Vladimirova, S.A. Powders Synthesized from Calcium Acetate and Mixed-Anionic Solutions, Containing Orthophosphate and Carbonate Ions, for Obtaining Bioceramic. *Glass Ceram.* **2018**, *75*, 118–123. [[CrossRef](#)]
46. Joksa, A.A.; Komarowska, L.; Ubele-Kalnina, D.; Viksna, A.; Gross, K.A. Role of carbonate on the crystallization and processing of amorphous calcium phosphates. *Materialia* **2023**, *27*, 101672. [[CrossRef](#)]
47. Glazov, I.E.; Krut'ko, V.K.; Musskaya, O.N.; Kulak, A.I. Low-Temperature Formation and Identification of Biphasic Calcium Carbonate Phosphates. *Russ. J. Inorg. Chem.* **2022**, *67*, 1718–1730. [[CrossRef](#)]
48. Ślósarczyk, A.; Paszkiewicz, Z.; Paluszkiwicz, C. FTIR and XRD evaluation of carbonated hydroxyapatite powders synthesized by wet methods. *J. Mol. Struct.* **2005**, *744*, 657–661. [[CrossRef](#)]
49. Peranidze, K.; Safronova, T.V.; Filippov, Y.; Kazakova, G.; Shatalova, T.; Rau, J.V. Powders Based on Ca₂P₂O₇–CaCO₃–H₂O System as Model Objects for the Development of Bioceramics. *Ceramics* **2022**, *5*, 423–434. [[CrossRef](#)]
50. Safronova, T.V.; Knot'ko, A.V.; Shatalova, T.B.; Evdokimov, P.V.; Putlyaev, V.I.; Kostin, M.S. Calcium phosphate ceramic based on powder synthesized from a mixed-anionic solution. *Glass Ceram.* **2016**, *73*, 25–31. [[CrossRef](#)]

51. Golubchikov, D.; Safronova, T.V.; Nemygina, E.; Shatalova, T.B.; Tikhomirova, I.N.; Roslyakov, I.V.; Khayrutdinova, D.; Platonov, V.; Boytsova, O.; Kaimonov, M.; et al. Powder Synthesized from Aqueous Solution of Calcium Nitrate and Mixed-Anionic Solution of Orthophosphate and Silicate Anions for Bioceramics Production. *Coatings* **2023**, *13*, 374. [CrossRef]
52. Zarga, Y.; Boubaker, H.B.; Ghaffour, N.; Elfil, H. Study of calcium carbonate and sulfate co-precipitation. *Chem. Eng. Sci.* **2013**, *96*, 33–41. [CrossRef]
53. Khayrutdinova, D.R.; Goldberg, M.A.; Antonova, O.S.; Kroklicheva, P.A.; Fomin, A.S.; Obolkina, T.O.; Konovalov, A.A.; Akhmedova, S.A.; Sviridova, I.K.; Kirsanova, V.A.; et al. Effects of Heat Treatment on Phase Formation in Cytocompatible Sulphate-Containing Tricalcium Phosphate Materials. *Minerals* **2023**, *13*, 147. [CrossRef]
54. Safronova, T.V.; Putlyaev, V.I.; Filippov, Y.; Shatalova, T.B.; Fatin, D.S. Ceramics based on brushite powder synthesized from calcium nitrate and disodium and dipotassium hydrogen phosphates. *Inorg. Mater.* **2018**, *54*, 195–207. [CrossRef]
55. Safronova, T.V. Phase composition of ceramic based on calcium hydroxyapatite powders containing byproducts of the synthesis reaction. *Glass Ceram.* **2009**, *66*, 136–139. [CrossRef]
56. Safronova, T.V.; Secheiko, P.A.; Putlyaev, V.I. Multiphase ceramics based on powders synthesized from sodium pyrophosphate and soluble calcium salts using mechanical activation. *Glass Ceram.* **2012**, *69*, 276–282. [CrossRef]
57. Safronova, T.V.; Putlyaev, V.I.; Kuznetsov, A.V.; Ketov, N.A.; Veresov, A.G. Properties of calcium phosphate powder synthesized from calcium acetate and sodium hydrophosphate. *Glass Ceram.* **2011**, *68*, 131–135. [CrossRef]
58. Safronova, T.V.; Steklov, M.Y.; Putlyaev, V.I.; Shekhirev, M.A. Na-substituted Ca-deficient carbonate hydroxyapatite for the production of ceramic materials. *Compos. Mater. Constr. (Konstr. Iz Kompoz. Mater.)* **2006**, *4*, 34–39. (In Russian)
59. Safronova, T.V.; Putlyaev, V.I.; Knot'ko, A.V.; Shatalova, T.B.; Artemov, M.V.; Filippov, Y.Y. Properties of Calcium Phosphate Powder Synthesized from Calcium Chloride and Potassium Pyrophosphate. *Inorg. Mater. Appl. Res.* **2020**, *11*, 44–49. [CrossRef]
60. Safronova, T.V.; Korneichuk, S.A.; Putlyaev, V.I.; Krut'ko, V.K. Ceramics based on calcium hydroxyapatite synthesized from calcium acetate, calcium hydroxide, and potassium hydrophosphate. *Glass Ceram.* **2012**, *69*, 30–36. [CrossRef]
61. Shiryaev, M.; Safronova, T.; Putlyaev, V. Calcium phosphate powders synthesized from calcium chloride and potassium hydrophosphate. *J. Therm. Anal. Calorim.* **2010**, *101*, 707–713. [CrossRef]
62. Safronova, T.V.; Shiryaev, M.A.; Putlyaev, V.I.; Murashov, V.A.; Protsenko, P.V. Ceramics based on hydroxyapatite synthesized from calcium chloride and potassium hydrophosphate. *Glass Ceram.* **2009**, *66*, 66–69. [CrossRef]
63. Aslanian, S.; Stoilova, D. Étude de l'ardealite, membre intermédiaire du système gypse-brushite. *Bull. De Minéralogie* **1982**, *105*, 621–624. [CrossRef]
64. Rinaudo, C.; Lanfranco, A.M.; Franchini-Angela, M. The system $\text{CaHPO}_4 \cdot 2\text{H}_2\text{O} - \text{CaSO}_4 \cdot 2\text{H}_2\text{O}$: Crystallizations from calcium phosphate solutions in the presence of SO_2 . *J. Cryst. Growth* **1994**, *142*, 184–192. [CrossRef]
65. Sakae, T.; Nagata, H.; Sudo, T. The crystal structure of synthetic calcium phosphate-sulfate hydrate, $\text{Ca}_2\text{HPO}_4 \cdot \text{SO}_4 \cdot 4\text{H}_2\text{O}$, and its relation to brushite and gypsum. *Am. Mineral.* **1978**, *63*, 520–527.
66. Pinto, A.J.; Carneiro, J.; Katsikopoulos, D.; Jiménez, A.; Prieto, M. The link between brushite and gypsum: Miscibility, dehydration, and crystallochemical behavior in the $\text{CaHPO}_4 \cdot 2\text{H}_2\text{O} - \text{CaSO}_4 \cdot 2\text{H}_2\text{O}$ system. *Cryst. Growth Des.* **2012**, *12*, 445–455. [CrossRef]
67. Moussa, H.; El Hadad, A.; Sarrigiannidis, S.; Saad, A.; Wang, M.; Taqi, D.; Tamimi, F. High toughness resorbable brushite-gypsum fiber-reinforced cements. *Mater. Sci. Eng. C* **2021**, *127*, 112205. [CrossRef]
68. Dumitraş, D.G. A re-investigation of ardealite from the type locality, the “dry” Cioclovina Cave (Şureanu Mountains, Romania). *Eur. J. Mineral.* **2017**, *29*, 1055–1066. [CrossRef]
69. Dumitraş, D.G.; Marincea, Ş. Sequential dehydration of the phosphate-sulfate association from Gura Dobrogei Cave, Dobrogea, Romania. *Eur. J. Mineral.* **2021**, *33*, 329–340. [CrossRef]
70. ICDD. *International Centre for Diffraction Data*; PDF-4+ 2010 (Database); Kabekkodu, S., Ed.; ICDD: Newtown Square, PA, USA, 2010; Available online: <https://www.icdd.com/pdf-2/> (accessed on 10 December 2022).
71. Nakamoto, K. *Infrared and Raman Spectra of Inorganic and Coordination Compounds*, 5th ed.; Wiley: New York, NY, USA, 1986; pp. 156–159.
72. Taherdangkoo, R.; Tian, M.; Sadighi, A.; Meng, T.; Yang, H.; Butscher, C. Experimental Data on Solubility of the Two Calcium Sulfates Gypsum and Anhydrite in Aqueous Solutions. *Data* **2022**, *7*, 140. [CrossRef]
73. Isa, K.; Okuno, H. Thermal decomposition of calcium sulfate dihydrate under self-generated atmosphere. *Bull. Chem. Soc. Jpn.* **1982**, *55*, 3733–3737. [CrossRef]
74. Frost, R.L.; Palmer, S.J.; Pogson, R. Thermal stability of the ‘cave’ mineral ardealite $\text{Ca}_2(\text{HPO}_4)(\text{SO}_4) \cdot 4\text{H}_2\text{O}$. *J. Therm. Anal. Calorim.* **2012**, *107*, 549–553. [CrossRef]
75. Ostroff, A.G.; Sanderson, R.T. Thermal stability of some metal sulphates. *J. Inorg. Nucl. Chem.* **1959**, *9*, 45–50. [CrossRef]
76. Collier, N.C. Transition and decomposition temperatures of cement phases—a collection of thermal analysis data. *Ceramics-Silikaty* **2016**, *60*, 338–343. [CrossRef]
77. Freyer, D.; Voigt, W. Crystallization and phase stability of CaSO_4 and CaSO_4 -based salts. *Mon. Für Chem./Chem. Mon.* **2003**, *134*, 693–719. [CrossRef]

-
78. Suchanek, W.; Yashima, M.; Kakihana, M.; Yoshimura, M. Hydroxyapatite ceramics with selected sintering additives. *Biomaterials* **1997**, *18*, 923–933. [[CrossRef](#)]
 79. Safronova, T.F.; Putlyaev, V.I.; Filippov, Y.Y.; Larionov, D.S.; Evdokimov, P.V.; Averina, A.E.; Klimashina, E.S.; Ivanov, V.K. Porous Ceramic Based on Calcium Pyrophosphate. *Refract. Ind. Ceram.* **2015**, *56*, 43–47. [[CrossRef](#)]

Disclaimer/Publisher’s Note: The statements, opinions and data contained in all publications are solely those of the individual author(s) and contributor(s) and not of MDPI and/or the editor(s). MDPI and/or the editor(s) disclaim responsibility for any injury to people or property resulting from any ideas, methods, instructions or products referred to in the content.